Electronic Suppplementary Information

Triarylboron-based TADF emitters with perfluoro substituents: high-efficiency OLEDs with a power efficiency over 100 lm W^{-1}

Ajay Kumar, [†a] Woochan Lee,[†b] Taehwan Lee,[a] Jaehoon Jung,*[a] Seunghyup Yoo,*[b] and Min Hyung Lee*[a]

[a] Department of Chemistry, University of Ulsan, Ulsan 44610, Republic of Korea
[b] School of Electrical Engineering, KAIST, Daejeon 34141, Republic of Korea

Contents

1. Experimental

1.1. General considerations

All synthetic procedures were carried out under an inert nitrogen atmosphere using standard Schlenk and glovebox techniques. Anhydrous-grade solvents (Aldrich) were dried over activated molecular sieves (5Å). Spectrophotometric-grade toluene and commercial reagents were used as received. 9-(2,5-(Dibromophenyl)-9*H*-carbazole (CzBr*o*Br)[1] and 9-(2-(dimesitylboryl)phenyl)-9*H*-carbazole (Cz*o*B, **1**)[2] were prepared according to the reported procedures. Deuterated solvents from Cambridge Isotope Laboratories were used. NMR spectra were recorded on a Bruker AM 300 (300.13 MHz for ^{1}H, 75.48 MHz for ^{13}C, 96.29 MHz for ^{11}B, and 282.38 MHz for ^{19}F) spectrometer at ambient temperature. Chemical shifts (in ppm) are reported against external Me_4Si (^{1}H, ^{13}C), $BF_3{\cdot}OEt_2$ (^{11}B), and $CFCl_3$ (^{19}F). Elemental analyses were performed on a Flash 2000 elemental analyzer (Thermo Scientific). Melting points (mp) were measured by Melting Point Apparatus SMP30 (Stuart Equipment). Thermogravimetric analysis (TGA) was performed with a TA Instruments Q50 under an N_2 atmosphere at a heating rate of 20 °C/min. Cyclic voltammetry experiments were carried out using an Autolab/PGSTAT101 system.

1.2. Synthesis

9-(2-Bromo-5-(trifluoromethyl)phenyl)-9*H*-carbazole (CzCF3*o*Br)

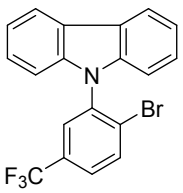

Sodium hydride (60% dispersion in mineral oil, 0.20 g, 4.94 mmol) was washed with *n*-hexane twice, dried, and dispersed in dry DMF (15 mL) under an nitrogen atmosphere. A solution of 9*H*-carbazole (0.83 g, 4.94 mmol) in dry DMF (10 mL) was slowly added to the suspension at room temperature. The mixture was stirred for 2 h and 1-bromo-2-fluoro-4-(trifluoromethyl)benzene (1.0 g, 4.12 mmol) in dry DMF (10 mL) was added to this solution. The mixture was heated at 120 °C overnight. After cooling down to room temperature, water (100 mL) was slowly added and a turbid white mixture was extracted with diethyl ether (50 mL × 3). The combined ether layer was washed with water (50 mL × 3). The organic layer was dried over $MgSO_4$, filtered, and concentrated under reduce pressure. The crude product was purified by silica gel column

chromatography using CH_2Cl_2/*n*-hexane (1:5, v/v) as an eluent to give CzCF3*o*Br as a white powder (yield: 1.45 g, 90%). ^{1}H NMR ($CDCl_3$): δ 8.19 (d, J = 7.8 Hz, 2H), 8.02 (d, J = 8.1 Hz, 1H), 7.81 (d, J = 2.1 Hz, 1H), 7.69 (dd, J = 8.4, 2.1 Hz, 1H), 7.45 (td, J = 7.6, 1.4 Hz, 2H), 7.35 (td, J = 7.5, 0.9 Hz, 2H), 7.08 (d, J = 8.1 Hz, 1H). ^{13}C NMR ($CDCl_3$): δ 140.4, 137.7, 135.0, 131.5 (q, J = 33.5 Hz), 128.1 (q, J = 3.8 Hz), 126.7 (q, J = 3.8 Hz), 126.2, 125.0, 123.5, 121.4, 120.5, 120.4, 109.8. ^{19}F NMR ($CDCl_3$): δ −63.5 (s). Anal. Calcd for $C_{19}H_{11}BrF_3N$: C, 58.48; H, 2.84; N, 3.59%. Found: C, 58.58; H, 2.93; N, 3.60%. mp = 122 °C.

3,6-Di-*tert*-butyl-9-(2-bromo-5-(trifluoromethyl)phenyl)-9*H*-carbazole (BuCzCF3*o*Br)

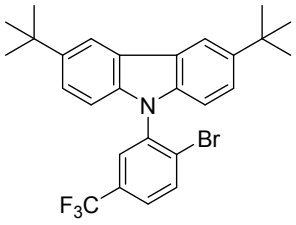

This compound was prepared in a manner analogous to the synthesis of CzCF3*o*Br using 3,6-di-*tert*-butyl-9*H*-carbazole to give BuCzCF3*o*Br as a white powder (yield: 0.73 g, 80%). ^{1}H NMR ($CDCl_3$): δ 8.20 (d, J = 1.8 Hz, 2H), 8.00 (d, J = 6.0 Hz, 1H), 7.75 (d, J = 2.1 Hz, 1H), 7.65 (dd, J = 8.4, 2.4 Hz, 1H), 7.49 (dd, J = 9.4, 1.9 Hz, 2H), 7.00 (d, J = 8.4 Hz, 1H), 1.45 (s, 18H, –C(CH_3)$_3$). ^{13}C NMR ($CDCl_3$): δ 143.4, 138.9, 138.3, 134.9 131.4 (q, J = 33.7 Hz), 128.7, 127.9 (q, J = 3.5 Hz), 127.8 (q, J = 1.8 Hz), 126.3 (q, J = 3.5 Hz), 125.1, 123.8, 123.5, 121.5, 116.5, 109.3, 34.7, 32.0 (–*C*(*C*H$_3$)$_3$). ^{19}F NMR ($CDCl_3$): δ −63.6 (s). Anal. Calcd for $C_{27}H_{27}BrF_3N$: C, 64.55; H, 5.42; N, 2.79%. Found: C, 64.41; H, 5.68; N, 2.76%. mp = 198 °C.

3,6-Di-*tert*-butyl-9-(2,5-dibromophenyl)-9*H*-carbazole (BuCzBr*o*Br)

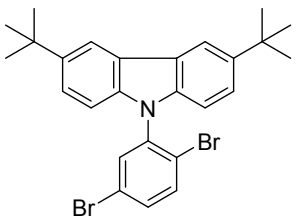

This compound was prepared in a manner analogous to the synthesis of CzBr*o*Br using 3,6-di-*tert*-butyl-9*H*-carbazole to give BuCzBr*o*Br as a white powder (yield: 3.24 g, 80%). ^{1}H NMR ($CDCl_3$): δ 8.13 (d, J = 1.5 Hz, 2H), 7.70 (d, J = 8.7 Hz, 1H), 7.57 (d, J = 2.1 Hz, 1H), 7.50 (dd, J = 8.4, 2.4 Hz, 1H), 7.46 (d, J = 1.8 Hz, 1H), 7.43 (d, J = 2.1 Hz, 1H), 7.00 (d, J = 8.7 Hz, 2H), 1.45 (s, 18H, –C(CH_3)$_3$). ^{13}C NMR ($CDCl_3$): δ 143.2, 139.0, 138.7, 135.2, 133.9, 132.8, 123.7, 123.4, 122.5, 121.5, 116.4, 109.4, 34.7, 32.0 (–*C*(*C*H$_3$)$_3$). Anal. Calcd for $C_{26}H_{27}Br_2N$: C, 60.84; H, 5.30; N, 2.73%. Found: C, 60.89; H, 5.31; N, 2.78%. mp = 236 °C.

9-(5-Bromo-2-(dimesitylboryl)phenyl)-9*H*-carbazole (CzBr*o*B)

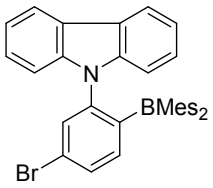

To a solution of 9-(2,5-dibromophenyl)-9*H*-carbazole (1.00 g, 2.49 mmol) in dry ether (50 mL) was added dropwise *n*-BuLi (1.0 mL, 2.50 mmol) at −78 °C. The reaction mixture was stirred at −78 °C for 1 h and then Mes_2BF (0.80 g, 2.99 mmol) in dry ether (10 mL) was slowly added. After stirring at room temperature overnight, the resulting yellow solution was quenched by the addition of a saturated aqueous NH_4Cl solution (50 mL), extracted with diethyl ether (30 mL × 3), and washed with water (50 mL). The combined organic layer was dried over $MgSO_4$, filtered, and concentrated under reduced pressure. The crude product was purified by silica gel column chromatography using CH_2Cl_2/*n*-hexane (1:10, v/v) as an eluent to give CzBr*o*B as a yellow powder (yield: 0.85 g, 60%). ^{1}H NMR ($CDCl_3$): δ 7.80 (d, J = 7.5 Hz, 2H), 7.69 (t, J = 1.8 Hz, 1H), 7.65 (d, J = 1.2 Hz, 1H), 7.60 (d, J = 7.8 Hz, 1H), 7.29–7.24 (m, 2H), 7.16–7.12 (m, 4H), 6.96–5.64 (br, 4H, Mes-*H*), 2.30–0.80 (br, 18H, Mes-CH_3). ^{13}C NMR ($CDCl_3$): δ 144.9, 143.9, 142.0, 140.5, 139.7, 133.5, 131.6, 127.9, 127.0, 124.8, 123.3, 119.4, 119.3, 110.2 (Ar–*C*), 23.7, 21.0 (–*C*H_3). ^{11}B NMR ($CDCl_3$): δ 76.9 (s, br). Anal. Calcd for $C_{36}H_{33}BBrN$: C, 75.81; H, 5.83; N, 2.46%; Found: C, 75.76; H, 5.77; N, 1.95%. mp = 186 °C.

3,6-Di-*tert*-butyl-9-(5-bromo-2-(dimesitylboryl)phenyl)-9*H*-carbazole (BuCzBr*o*B)

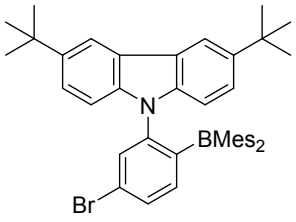

This compound was prepared in a manner analogous to the synthesis of CzBr*o*B using 3,6-di-*tert*-butyl-9*H*-carbazole to give BuCzBr*o*B as a yellow powder (yield: 0.90 g, 65%). ^{1}H NMR ($CDCl_3$): δ 7.80 (s, 2H), 7.70 (d, J = 1.8 Hz, 1H), 7.65 (dd, J = 8.1, 1.8 Hz, 1H), 7.60 (d, J = 8.1 Hz, 1H), 7.34 (dd, J = 8.4, 1.8 Hz, 2H), 7.12 (d, J = 9.3 Hz, 2H), 6.75 (s, br, 2H, Mes–*H*), 5.91 (s, br, 2H, Mes–*H*), 2.04–1.80 (br, 18H, Mes–CH_3), 1.45 (s, 18H, –C(CH_3)$_3$). ^{13}C NMR ($CDCl_3$): δ 144.6, 142.2, 139.9, 133.2, 131.2, 128.3, 127.1, 123.2, 122.4, 115.2, 109.5 (Ar–*C*), 34.6, 32.1 (–*C*(*C*H_3)$_3$), 23.9, 21.1 (Mes–*C*H_3). ^{11}B NMR ($CDCl_3$): δ 82.2 (s, br).). Anal. Calcd for $C_{44}H_{49}BBrN$: C, 77.42; H, 7.24; N, 2.05%. Found: C, 77.43; H, 7.22; N, 2.13%. mp = 216 °C.

9-(2-(Dimesitylboryl)-5-(trifluoromethyl)phenyl)-9*H*-carbazole (CzCF3*o*B, 2)

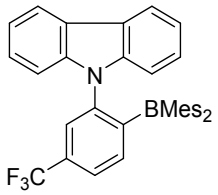

To a solution of CzCF3*o*Br (0.50 g, 1.28 mmol) in dry ether (50 mL) was added dropwise *n*-BuLi (0.56 mL, 1.41 mmol) at −78 °C. The reaction mixture was stirred at −78 °C for 1 h and then Mes_2BF (0.38 g, 1.41 mmol) in dry ether (10 mL) was slowly added. After stirring at room temperature overnight, the resulting solution was quenched by the addition of a saturated aqueous NH_4Cl solution (50 mL), extracted with diethyl ether (30 mL × 3), and washed with water (100 mL). The combined organic layer was dried over $MgSO_4$, filtered, and concentrated under reduced pressure. The crude product was purified by silica gel column chromatography using CH_2Cl_2/*n*-hexane (1:20, v/v) as an eluent to give CzCF3*o*B as a yellow powder (yield: 0.48 g, 68%). Single crystals suitable for an X-ray diffraction study were grown from a solution of CzCF3*o*B in CH_3OH/CH_2Cl_2. ^{1}H NMR ($CDCl_3$): δ 7.85−7.72 (m, 5H), 7.24 (td, J = 7.6, 1.2 Hz, 2H), 7.14 (d, J = 7.2 Hz, 2H), 7.08 (t, J = 7.6, 2H), 6.31 (br, 4H, Mes-*H*), 2.23−1.31 (br, 18H, Mes-CH_3). ^{13}C NMR ($CDCl_3$): δ 143.2, 142.1, 140.4, 138.8, 134.4 (q, J = 33.0 Hz), 128.0, 127.2 (q, J = 3.5 Hz), 125.3, 124.8 (q, J = 4.0 Hz), 123.3, 121.7, 119.5, 119.4, 110.0 (Ar–*C*), 23.3, 21.0 (–*C*H_3). ^{11}B NMR ($CDCl_3$): δ 78.8 (s, br). ^{19}F NMR ($CDCl_3$): δ −99.5 (s). Anal. Calcd for $C_{37}H_{33}BF_3N$: C, 79.43; H, 5.95; N, 2.50%. Found: C, 79.37; H, 5.98; N, 2.57%. mp = 164 °C. T_{d5} = 248 °C.

9-(2-(Dimesitylboryl)-5-(perfluoropropyl)phenyl)-9*H*-carbazole (CzCF7*o*B, 3)

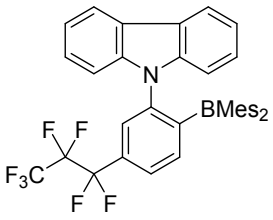

Freshly precipitated copper powder (0.28 g, 4.4 mmol) was taken in a Schlenk flask and dried under vaccum for 2 h. A solution of CzBr*o*B (0.50 g, 0.88 mmol) and heptafluoropropyl iodide (0.29 g, 0.97 mmol) in dry DMF (10 ml) was added to the Schlenk flask. The resulting mixture was stirred at 110 °C for 24 h. After cooling down to room temperature, water (100 mL) was slowly added and extracted with diethyl ether (50 mL × 3). The combined ether layer was washed with water (50 mL × 3). The organic layer was dried over $MgSO_4$, filtered, and concentrated under reduce pressure. The crude product was purified by silica gel column chromatography using CH_2Cl_2/*n*-hexane (1:20, v/v) as an eluent to give CzCF7*o*B as a yellowish green powder (yield: 0.38 g, 65%). ^{1}H NMR ($CDCl_3$): δ 7.85 (d, J = 7.8 Hz, 1H), 7.83 (d, J = 7.8 Hz, 2H), 7.71 (m, 2H), 7.24 (dt, J = 7.6, 1.2 Hz, 2H), 7.13 (t, J = 7.2 Hz, 2H), 7.05(d, J = 7.8, 2H),

6.31 (br, 4H, Mes-*H*), 2.05–1.31 (br, 18H, Mes-CH_3). ^{13}C NMR ($CDCl_3$): δ 143.1, 142.1, 140.4, 138.5, 132.6 (t, J = 25.3 Hz), 128.7 (t, J = 6.4 Hz), 128.1, 126.2 (t, J = 6.0 Hz), 125.0, 123.4, 119.5, 119.4, 110.0 (Ar–*C*), 23.3, 21.0 (–*C*H_3). ^{11}B NMR ($CDCl_3$): δ 80.0 (s, br). ^{19}F NMR ($CDCl_3$): δ −80.9 (t, J = 9.0 Hz), −113.2 (q, J = 8.8 Hz), −127.5 (s). Anal. Calcd for $C_{39}H_{33}BF_7N$: C, 71.03; H, 5.04; N, 2.12%. Found: C, 71.24; H, 5.04; N, 2.35%. mp = 85 °C. T_{d5} = 258 °C.

9-(2-(Dimesitylboryl)-5-(*p*-perfluorotolyl)phenyl)-9*H*-carbazole (CzTF7*o*B, 4)

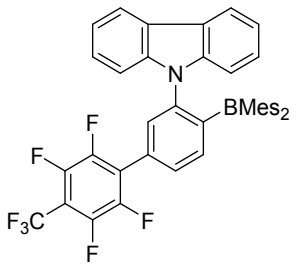

To a solution of CzBr*o*B (0.5 g, 0.88 mmol) in dry ether (50 mL) was added dropwise *n*-BuLi (0.42 mL, 1.05 mmol) at −78 °C. The reaction mixture was stirred at −78 °C for 1 h and then octafluorotoluene (0.25 g, 1.05 mmol) in dry ether (10 mL) was slowly added. After stirring at room temperature overnight, the resulting dark green solution was quenched by the addition of a saturated aqueous NH_4Cl solution (50 mL), extracted with diethyl ether (30 mL × 3), and washed with water (50 mL). The combined organic layer was dried over $MgSO_4$, filtered, and concentrated under reduced pressure. The crude product was purified by silica gel column chromatography using CH_2Cl_2/*n*-hexane (1:5, v/v) as an eluent to give CzTF7*o*B as a yellow powder (yield: 0.47 g, 75%). ^{1}H NMR ($CDCl_3$): δ 7.89 (d, J = 7.8 Hz, 1H), 7.83 (d, J = 7.8 Hz,2H), 7.70–7.62 (m, 2H), 7.31–7.24 (m, 2H), 7.21–7.14 (m, 4H), 6.35 (br, 4H, Mes-*H*), 2.50–1.15 (br, 18H, Mes-CH_3). ^{13}C NMR ($CDCl_3$): δ 145.0, 146.2 (C–F splitting was not clearly observed), 145.8 (C–F splitting was not clearly observed), 144.0, 143.3, 142.2, 140.6, 139.7, 138.8, 133.6, 131.8, 131.6, 130.3, 129.6, 128.0, 127.0, 125.0, 123.4, 119.6, 119.4, 110.2 (Ar–*C*), 23.6, 21.1 (–*C*H_3). ^{11}B NMR ($CDCl_3$): δ 83.8 (s, br). ^{19}F NMR ($CDCl_3$): δ −57.2 (t, J = 21.5 Hz), −140.6 (m), −141.7 (m). Anal. Calcd for $C_{43}H_{33}BF_7N$: C, 73.00; H, 4.70; N, 1.98%. Found: C, 72.81; H, 4.71; N, 2.04%. mp = 210 °C. T_{d5} = 310 °C.

3,6-Di-*tert*-butyl-9-(2-(dimesitylboryl)-5-(trifluoromethyl)phenyl)-9*H*-carbazole (BuCzCF3*o*B, 5)

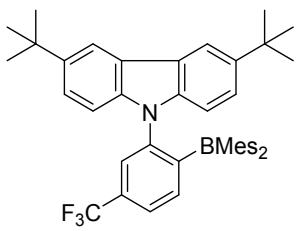

This compound was prepared in a manner analogous to the synthesis of CzCF3*o*B (**2**) using BuCzCF3*o*Br to give BuCzCF3*o*B as a yellow powder (yield: 0.37 g, 55%). Single crystals suitable for an X-ray diffraction study

were grown from a solution of BuCzCF3*o*B in CH_3OH/CH_2Cl_2. ^{1}H NMR ($CDCl_3$): δ 7.86–7.71 (m, 5H), 7.31 (dd, J = 8.7, 1.8 Hz, 2H), 7.05 (d, J = 8.7 Hz, 2H), 6.32 (br, 4H, Mes-*H*), 2.16–1.28 (br, 18H, Mes-CH_3), 1.45 (s, 18H, –C(CH_3)$_3$). ^{13}C NMR ($CDCl_3$): δ 149.4, 143.9, 142.3, 140.6, 140.0, 134.5 (q, J = 33.0 Hz), 127.9, 126.9 (q, J = 3.5 Hz), 125.4, 124.4 (q, J = 3.7 Hz), 123.3, 122.5, 121.8, 115.3, 109.4 (Ar–*C*), 34.6, 32.1 (–*C*(*C*H$_3$)$_3$), 23.7, 21.1 (Mes–*C*H$_3$). ^{11}B NMR ($CDCl_3$): δ 80.8 (s, br). ^{19}F NMR ($CDCl_3$): δ −63.8 (s). Anal. Calcd for $C_{45}H_{49}BF_7N$: C, 80.47; H, 7.35; N, 2.09%. Found: C, 80.26; H, 7.33; N, 2.24%. mp = 218 °C. T_{d5} = 305 °C.

3,6-Di-*tert*-butyl-9-(2-(dimesitylboryl)-5-(perfluoropropyl)phenyl)-9*H*-carbazole (BuCzCF7*o*B, 6)

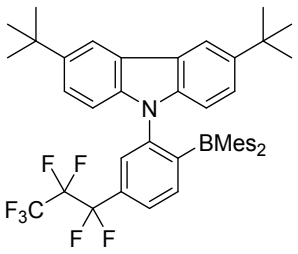

This compound was prepared in a manner analogous to the synthesis of CzCF7*o*B (**3**) using BuCzBr*o*B to give BuCzCF7*o*B as a yellow powder (yield: 0.35 g, 62%). ^{1}H NMR ($CDCl_3$): δ 7.84 (d, J = 7.8 Hz, 1H), 7.77–7.72 (m, 3H), 7.66 (d, J = 8.1 Hz, 1H), 7.30 (dd, J = 8.6, 2.0 Hz, 2H), 7.01 (d, J = 8.7 Hz, 1H), 6.65–5.98 (br, 4H, Mes-*H*), 2.15–1.50 (br, 36H, Mes-CH_3, –C(CH_3)$_3$). ^{13}C NMR ($CDCl_3$): δ 149.7, 143.8, 143.6, 142.4, 140.7, 138.8, 132.9 (t, J = 24.5 Hz), 128.5 (t, J = 6.0 Hz), 128.1, 125.9 (t, J = 6.0 Hz), 123.4, 122.7, 115.54, 109.3 (Ar–*C*), 34.7, 32.1 (–*C*(*C*H$_3$)$_3$), 23.2, 21.2 (Mes–*C*H$_3$). ^{11}B NMR ($CDCl_3$): δ 84.8 (s, br). ^{19}F NMR ($CDCl_3$): δ −80.9 (t, J = 9.0 Hz), −113.3 (q, J = 8.5 Hz), −127.6 (s). Anal. Calcd for $C_{47}H_{49}BF_7N$: C, 73.15; H, 6.40; N, 1.82%. Found: C, 73.17; H, 6.42; N, 2.05%. mp = 124 °C. T_{d5} = 286 °C.

3,6-Di-*tert*-butyl-9-(2-(dimesitylboryl)-5-(*p*-perfluorotolyl)phenyl)-9*H*-carbazole (BuCzTF7*o*B, 7)

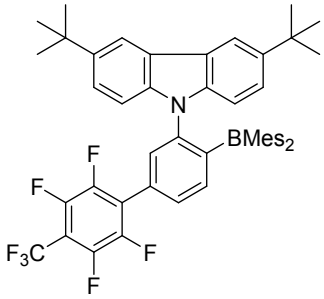

This compound was prepared in a manner analogous to the synthesis of CzTF7*o*B (**4**) using BuCzBr*o*B to give BuCzTF7*o*B as a yellow powder (yield: 0.44 g, 73%). ^{1}H NMR ($CDCl_3$): δ 7.91 (d, J = 7.8 Hz, 1H), 7.84 (s, 2H), 7.69 (s, 1H), 7.63 (dd, J = 7.9, 1.4 Hz, 1H), 7.68 (dd, J = 8.4, 1.8 Hz, 2H), 7.21 (t, J = 8.6, 2H), 7.01–5.32 (br, 4H, Mes-*H*), 2.62–1.12 (br, 36H, Mes-CH_3, –C(CH_3)$_3$). ^{13}C NMR ($CDCl_3$): δ 147.1, 146.1 (C–F splitting was not clearly observed), 145.9, 145.6 (C–F splitting was not clearly observed), 143.9, 142.3, 140.6, 139.0, 131.4, 130.3, 129.1, 127.9,

123.6, 123.3, 122.6, 115.2, 109.4 (Ar–*C*), 34.6, 32.1 (–*C*(*C*H$_3$)$_3$), 23.8, 21.2 (Mes–*C*H$_3$). ^{11}B NMR ($CDCl_3$): δ 84.3 (s, br). ^{19}F NMR ($CDCl_3$): δ −57.2 (t, J = 21.5 Hz), −140.6 (m), −141.6 (m). Anal. Calcd for $C_{51}H_{49}BF_7N$: C, 74.72; H, 6.03; N, 1.71%. Found: C, 74.65; H, 6.03; N, 1.85%. mp = 234 °C. T_{d5} = 321 °C.

1.3. X-ray Crystallography

Single crystals of suitable size and quality (CzCF3*o*B, **2** and BuCzCF3*o*B, **5**) were coated with Paratone oil and mounted onto a glass capillary. Diffractrion data were obtained at 173 K. The crystallographic measurements were performed on a Bruker SMART Apex II CCD area detector diffractometer with a graphite-monochromated Mo-Kα radiation (λ = 0.71073 Å). The structures were solved by direct methods[3] and refined by full-matrix least-squares fitting on F^2 using SHELXL-2014.[4] All non-hydrogen atoms were refined with anisotropic displacement parameters. The carbon-bound hydrogen atoms were introduced at calculated positions and all hydrogen atoms were treated as riding atoms with an isotropic displacement parameter equal to 1.2 times that of the parent atom. Full details of the structure determinations have been deposited as a cif with the Cambridge Crystallographic Data Collection under CCDC deposition numbers 1907673 and 1907693 (**2** and **5**). The data can be obtained free of charge via www.ccdc.cam.ac.uk/data_request/cif.

1.4. Cyclic Voltammetry

Cyclic voltammetry measurements were carried out in DMF (1×10^{-3} M) with a three-electrode cell configuration consisting of platinum working and counter electrodes and an $Ag/AgNO_3$ (0.01 M in CH_3CN) reference electrode at room temperature. Tetra-*n*-butylammonium hexafluorophosphate (0.1 M) was used as the supporting electrolyte. The redox potentials were recorded at a scan rate of 200 mV/s and are reported with reference to the ferrocene/ferrocenium (Fc/Fc^+) redox couple.

1.5. Photophysical Measurements

The UV/vis absorption and photoluminescence (PL) spectra were recorded on a Varian Cary 100 and FS5 spectrophotometer, respectively. Solution PL spectra were obtained from oxygen-free and air-saturated toluene solutions (typically 20 μM in toluene). The doped host film samples for PL spectra and PLQYs were prepared on quartz plates. PLQYs of all samples were measured on an absolute PL quantum yield spectrophotometer (Quantaurus-QY C11347-11, Hamamatsu Photonics) equipped with a 3.3-inch integrating sphere. Transient PL decays were measured on a FS5 spectrophotometer (Edinburgh Instruments) in either time-correlated single-photon counting (TCSPC) mode (with an EPL-375 ps pulsed diode laser as a light source) or multichannel scaling (MCS) mode (with a microsecond xenon flashlamp as a light source). The lifetimes of prompt fluorescence (τ_p) were estimated by fitting decay curves measured via the TCSPC mode, while those of delayed fluorescence (τ_d) were estimated with curves measured via the MCS mode. The temperature dependence of PL decay was obtained with an OptistatDN^{TM} cryostat (Oxford Instruments). The HOMO and LUMO energy levels were determined from the electrochemical oxidation and reduction (E_{onset} or $E_{1/2}$) peaks of cyclic voltammograms.

1.6. Theoretical Calculations

The computational study based on the density functional theory (DFT) was carried out to elucidate the structural, electronic, and photophyscial properties. The PBE0 hybrid functional[5] and 6-31G(d,p) basis set implemented in GAUSSIAN 16 software package[6] were used. In order to improve the reliability of computational result, we also employed B3LYP functional[7] of which data qualitatively agreed well with those obtained with PBE0 functional and are provided in parentheses of Tables S4–S6. The ground (S_0) states of compounds were optimized using DFT calculations, and their lowest singlet (S_1) and triplet (T_1) excited states were optimized using time-dependent DFT (TD-DFT) calculations with the same functional and basis set. The polarizable continuum model using the integral equation formalism (IEFPCM) was employed to take account for the influence of solvent medium (toluene).[8] The composition of frontier molecular orbital and the overlap integral extents were computed using AOMix[9] and Multiwfn[10] programs, respectively.

1.7. Fabrication of Electroluminescent Devices

The configuration of the fabricated TADF-OLEDs is depicted in **Figure S19**: glass/indium-tin-oxide (ITO) (70 or 150 nm)/poly(3,4-ethylenedioxy-thiophene):poly(styrenesulfonate) (PEDOT:PSS) (40 nm)/1,1-bis[(di-4-tolylamino)phenyl]cyclohexane (TAPC) (20 nm)/4,4',4"-tris(carbazol-9-yl)triphenylamine (TCTA) (10 nm)/TCTA:4,6-bis(3,5-di-3-pyridylphenyl)-2-methylpyrimidine (B3PYMPM):emitter (20 wt%, 15 nm)/B3PYMPM (55 nm)/LiF (1 nm)/Al (100 nm). Glass substrates with pre-patterned ITO electrodes were cleaned by a sequential wet-cleaning processes in an ultrasonic bath.[11] After drying in a vacuum oven for a day, the substrates were subject to air plasma treatment for 1 min in a plasma cleaner (CUTE-MP, Femto Science). As a hole-injection layer, an aqueous dispersion of PEDOT:PSS (Clevios^{TM} P VP AI 4083, Heraeus) was spun (2500 rpm for 30 s) onto the plasma-treated substrates and annealed on a hot plate (100 °C for 10 min). Other organic and metal layers were sequentially deposited in a vacuum chamber (HS-1100, Digital Optics & Vacuum) at less than 2×10^{-6} torr. The current density–voltage–luminance (*J–V–L*) and angle-resolved electroluminescence (EL) intensity characteristics of the fabricated devices were obtained with a source-measure unit (Keithley 2400) using a calibrated photodiode (FDS100, Thorlab) and a fiber optic spectrometer (EPP2000, StellarNet) held on a motorized goniometer. The EQE (η_{EQE}) and PE (η_{PE}) of the devices were estimated from the measured full angular characteristics without Lambertian simplification. All device fabrication and measurement, except for the PEDOT:PSS coating, were carried out in a nitrogen (N_2)-filled glove box, and all characteristics of the devices were measured at room temperature.

1.8. Optical Simulation

For optical analysis, a simulation was carried out using a power dissipation model, that is, coherent dipole ratio theory. The simulation was performed on the basis of an advanced classical dipole model that considers the Purcell effect, dipole orientation, and coupling to waveguide modes and surface plasmon polariton (SPP) modes.[12] The refractive indices of the materials used in the simulation were

obtained by spectroscopic ellipsometry. We assumed that electrical loss was negligible and hole-electron charge balancing was equal to unity. The measured Φ_{PL} of 0.87 for the doped host film of **5** was used in the simulation.

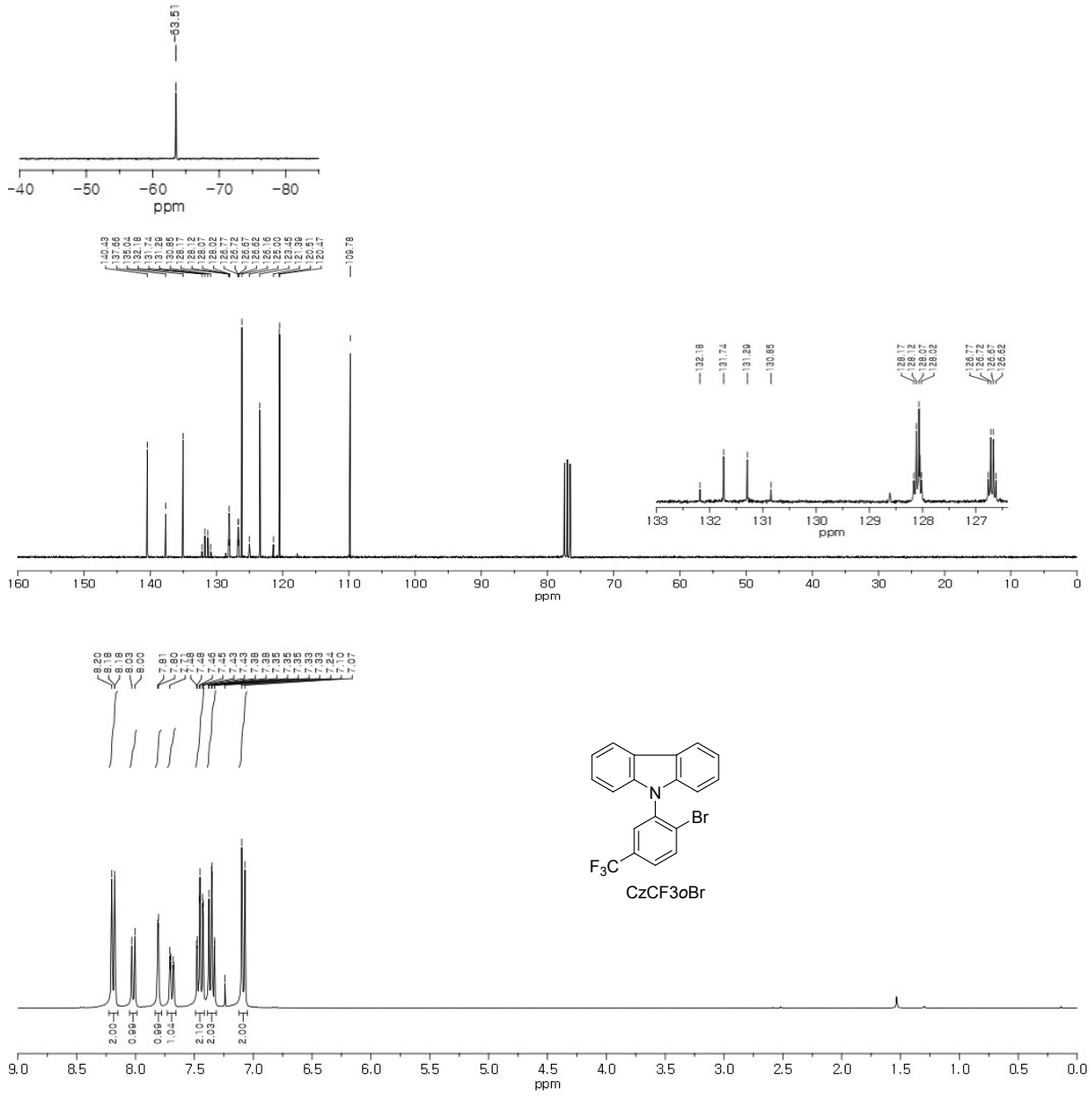

Figure S1. ^{1}H (bottom), ^{13}C (middle), and ^{19}F (top) NMR spectra of CzCF3*o*Br in $CDCl_3$.

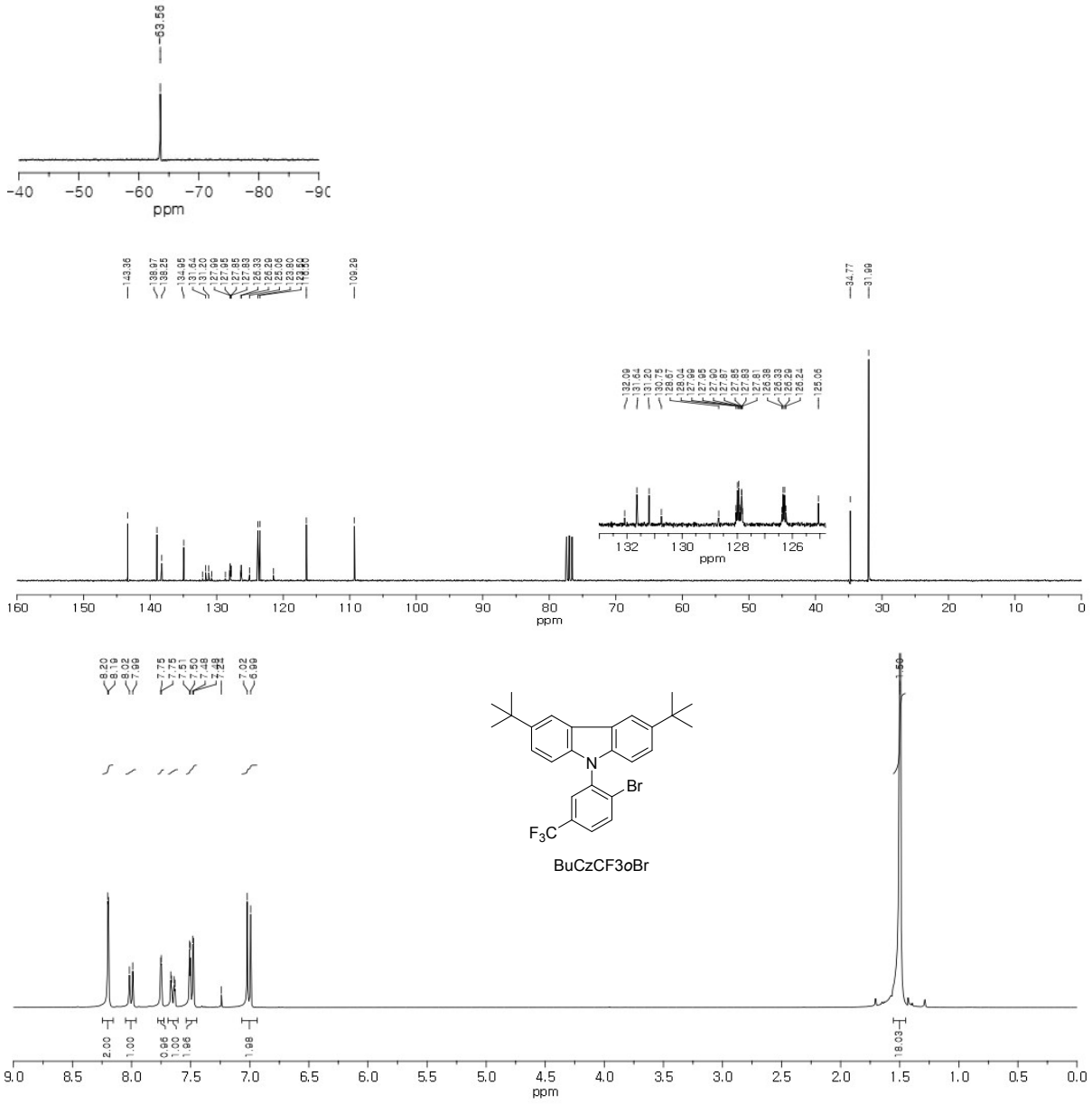

Figure S2. ^{1}H (bottom), ^{13}C (middle), and ^{19}F (top) NMR spectra of BuCzCF3*o*Br in $CDCl_3$.

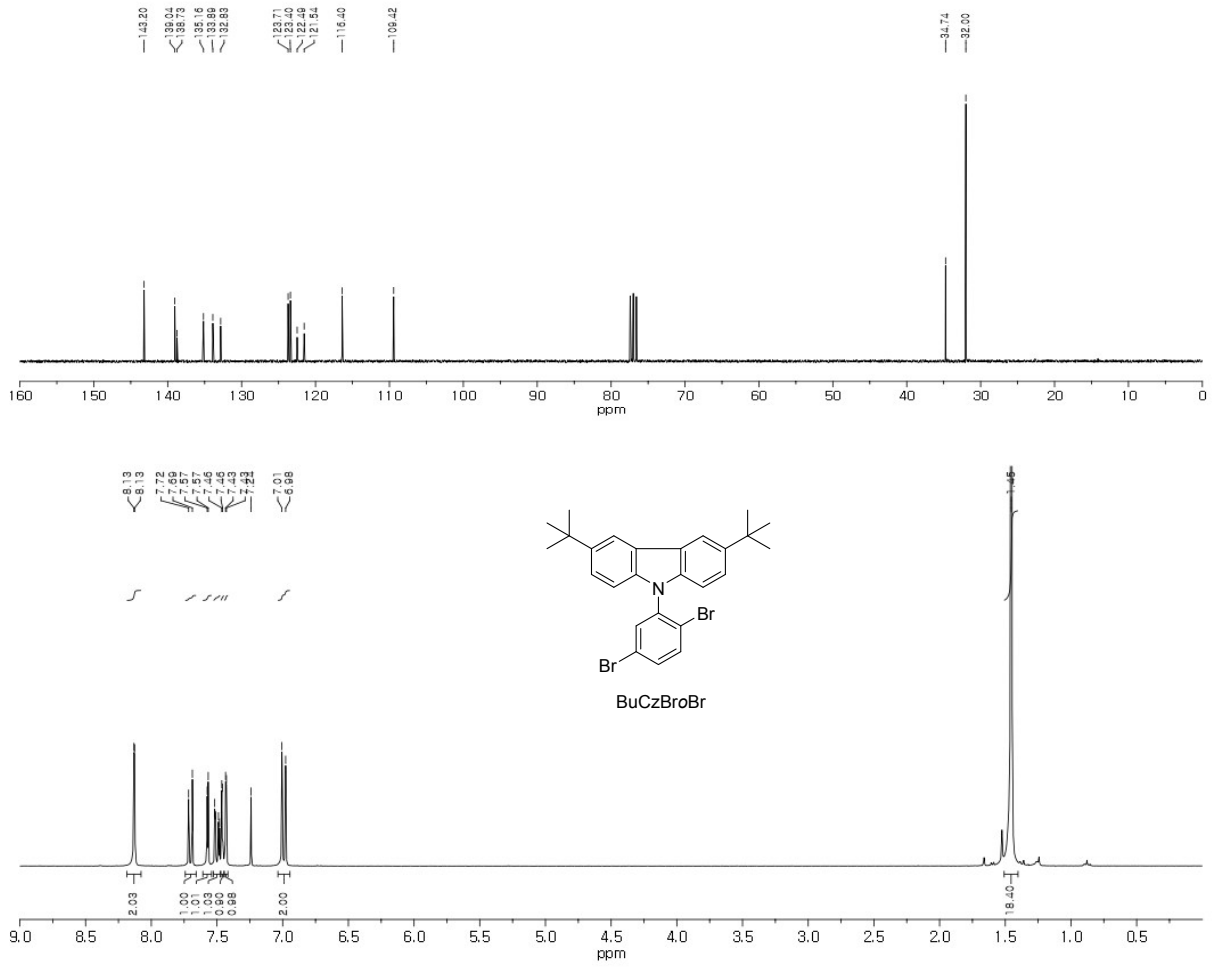

Figure S3. ^{1}H (bottom) and ^{13}C (top) NMR spectra of CzBr*o*Br in $CDCl_3$.

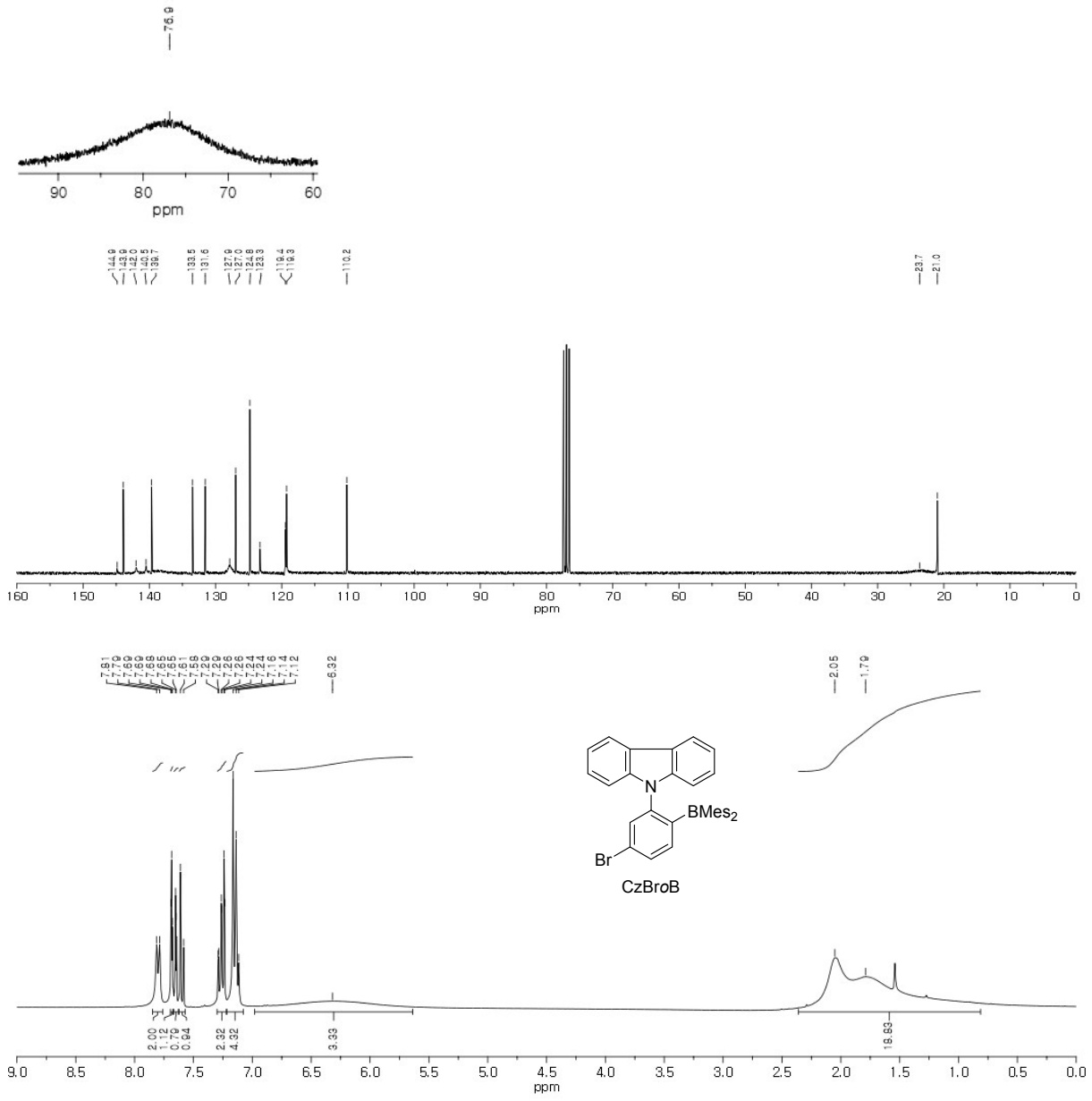

Figure S4. ^{1}H (bottom), ^{13}C (middle), and ^{11}B (top) NMR spectra of CzBr*o*B in $CDCl_3$.

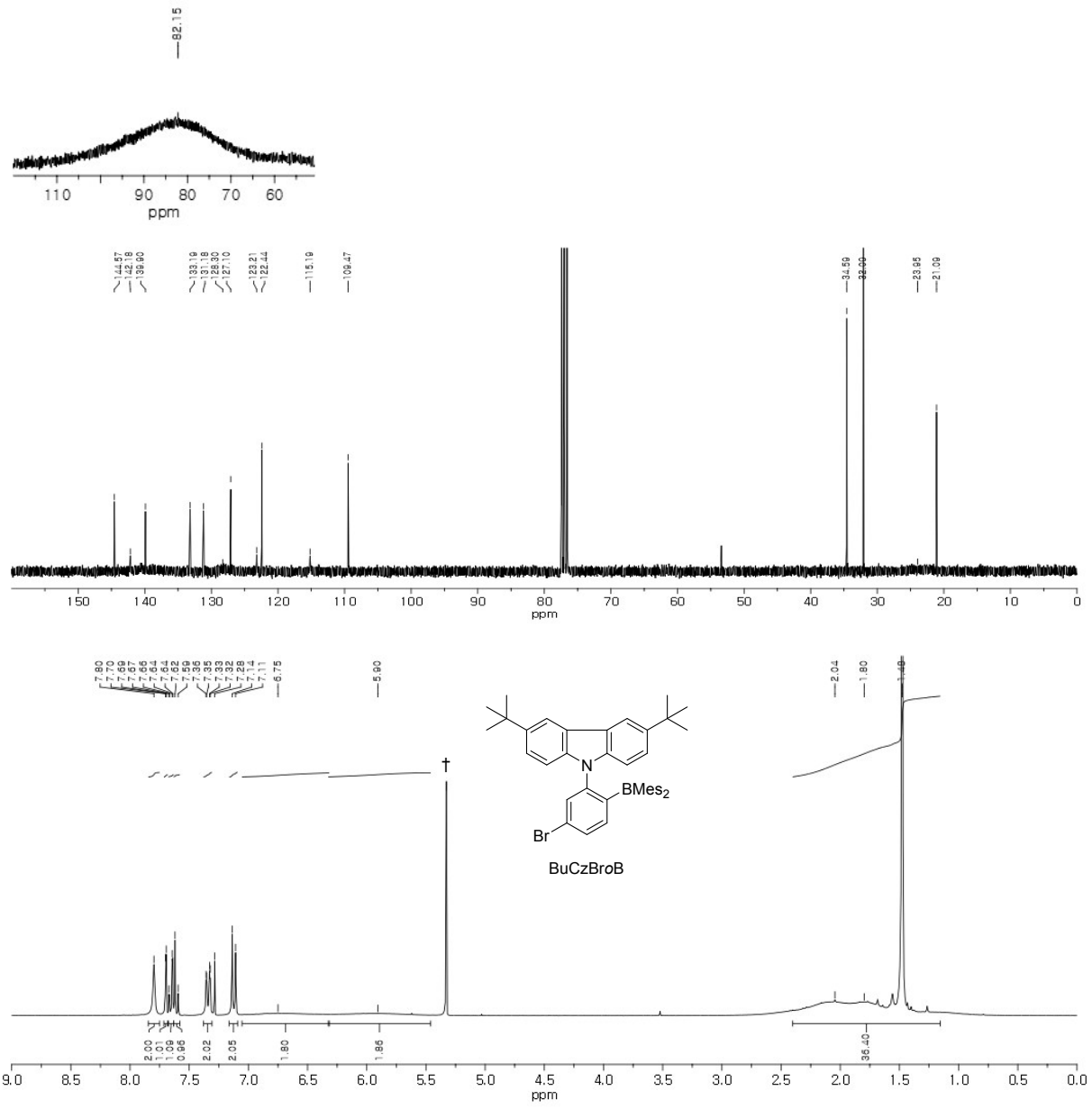

Figure S5. ^{1}H (bottom), ^{13}C (middle), and ^{11}B (top) NMR spectra of BuCzBr*o*B in $CDCl_3$ († from residual CH_2Cl_2).

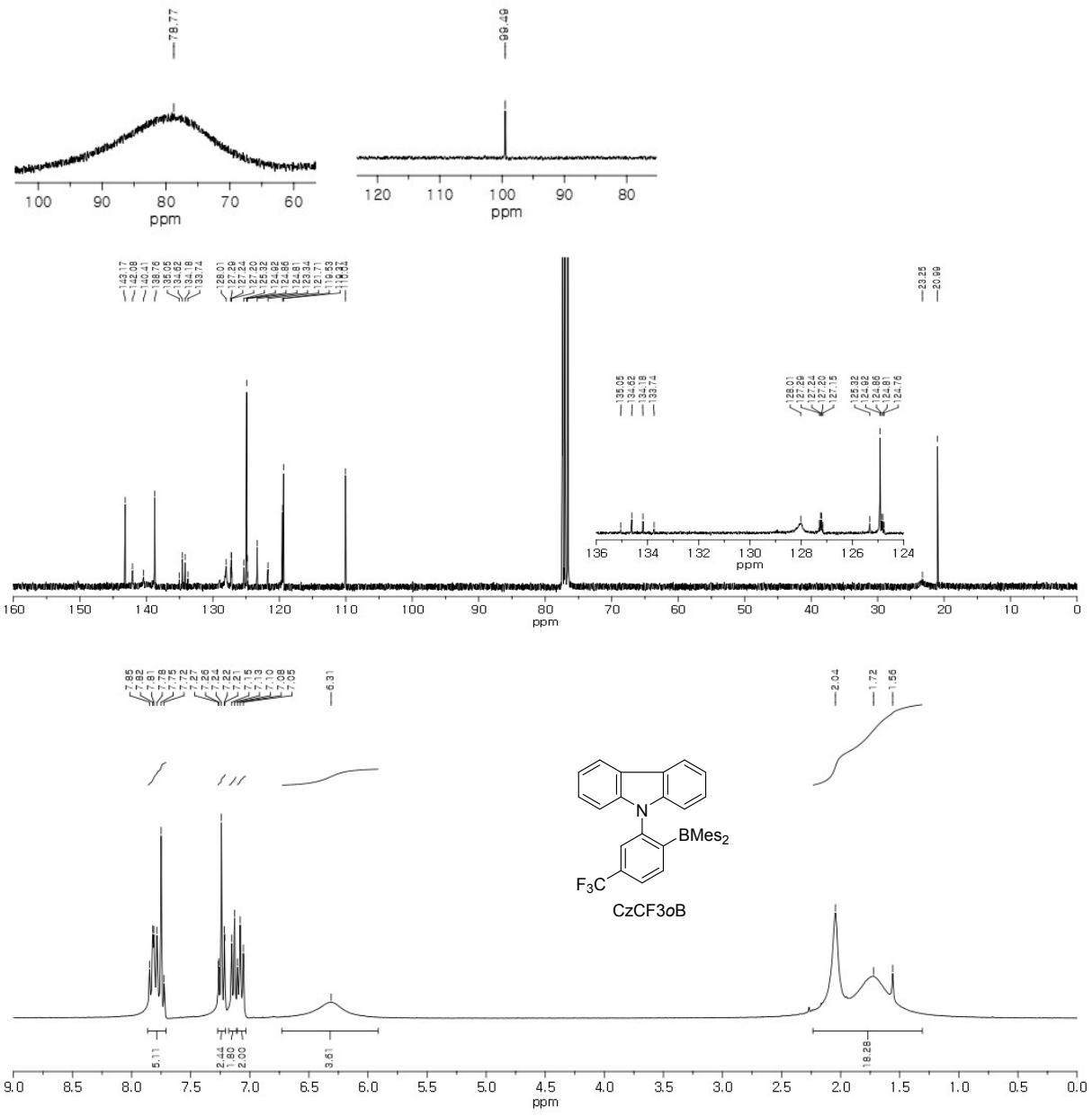

Figure S6. ^{1}H (bottom), ^{13}C (middle), ^{11}B (top left), and ^{19}F (top right) NMR spectra of CzCF3*o*B (**2**) in $CDCl_3$.

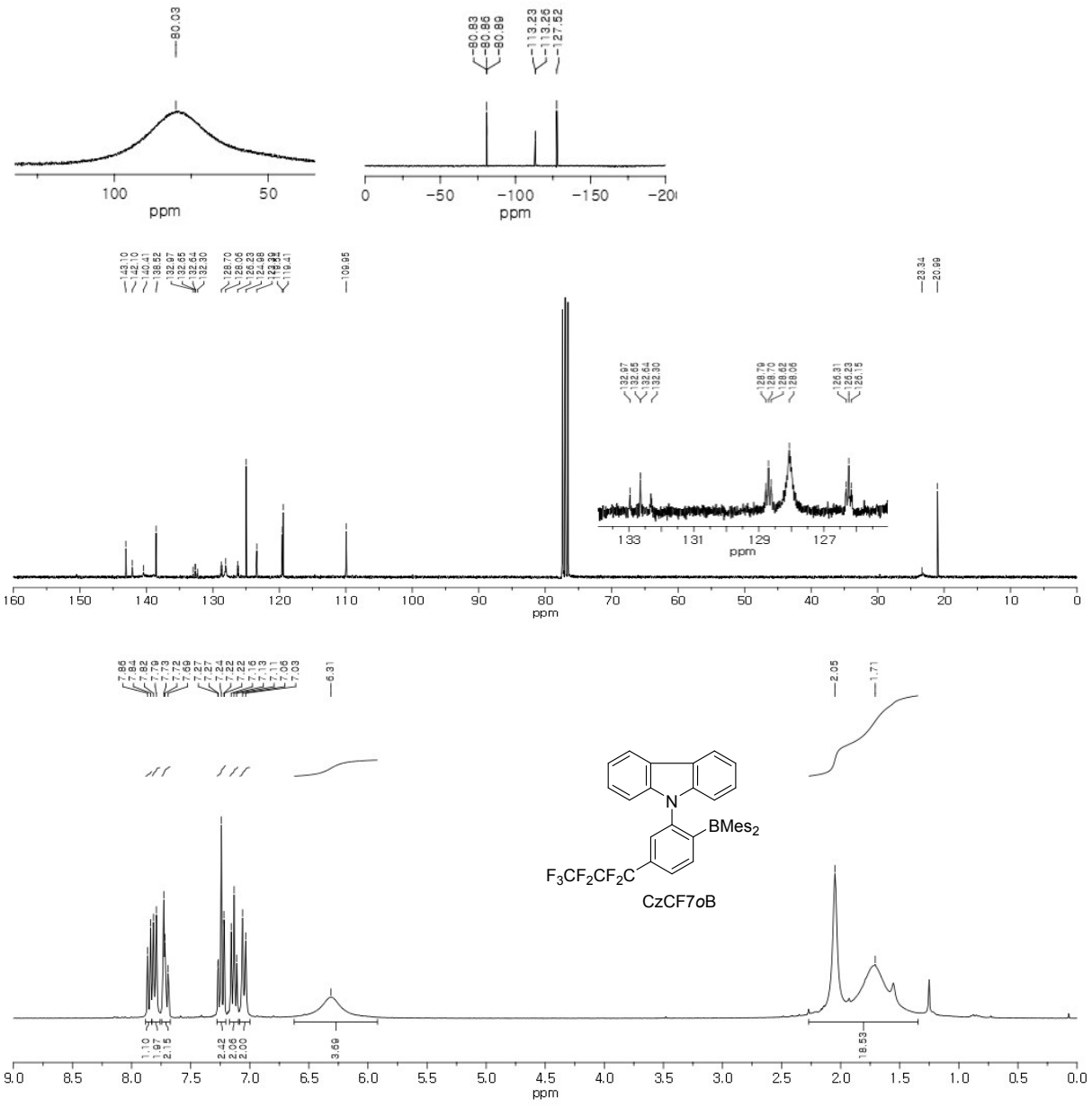

Figure S7. ^{1}H (bottom), ^{13}C (middle), ^{11}B (top left), and ^{19}F (top right) NMR spectra of CzCF7*o*B (**3**) in $CDCl_3$.

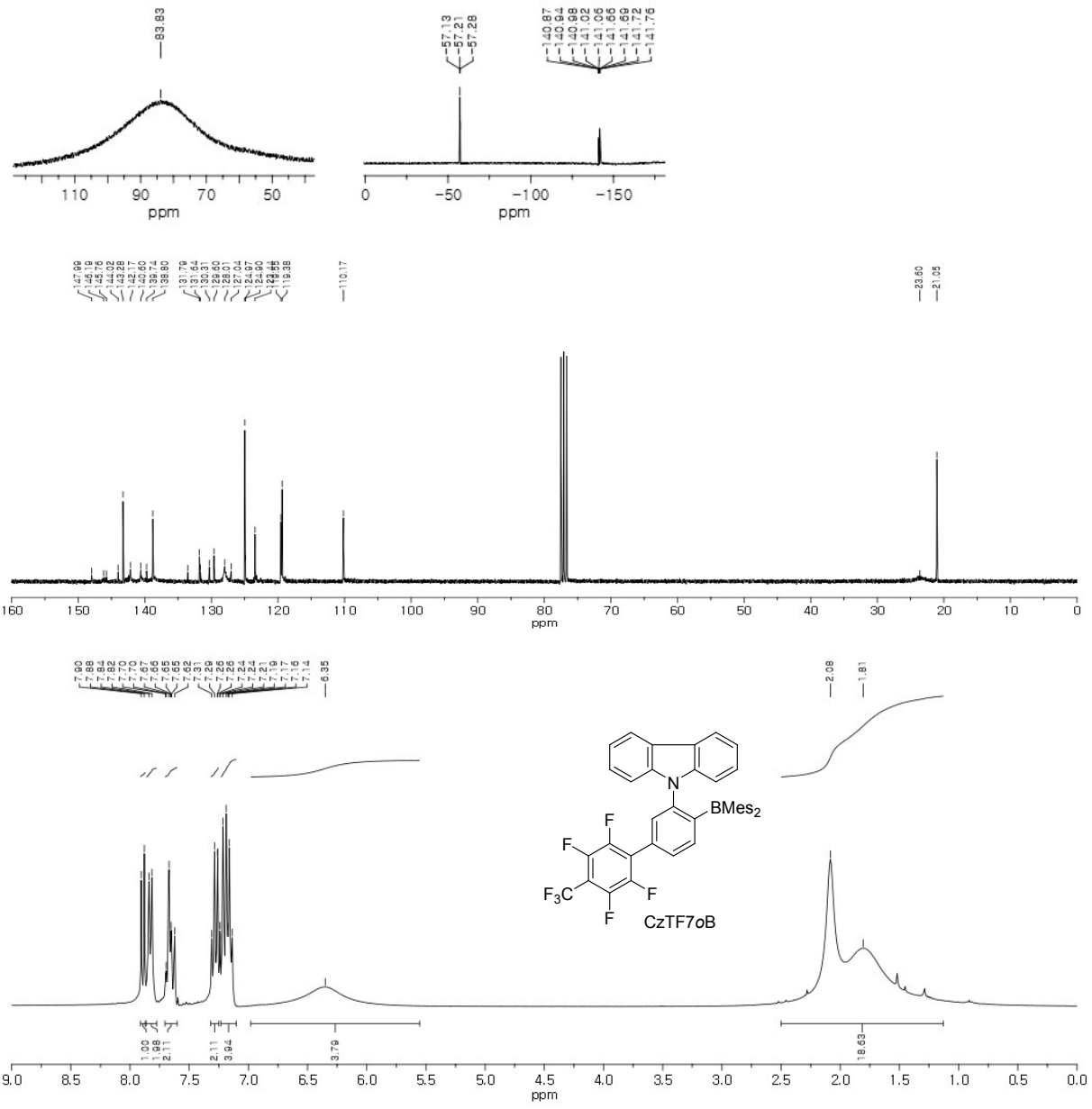

Figure S8. ^{1}H (bottom), ^{13}C (middle), ^{11}B (top left), and ^{19}F (top right) NMR spectra of CzTF7*o*B (**4**) in $CDCl_3$.

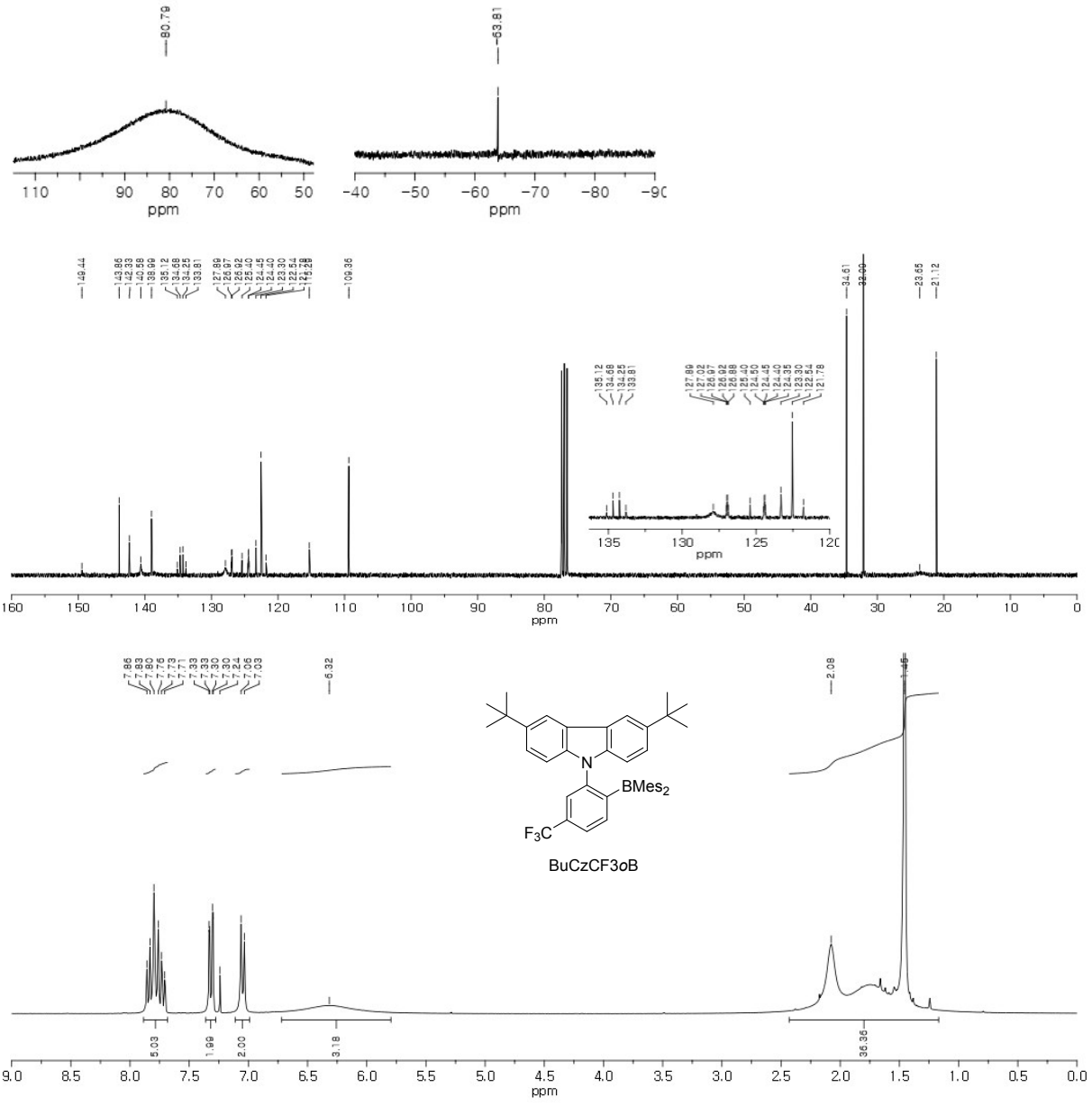

Figure S9. ^{1}H (bottom), ^{13}C (middle), ^{11}B (top left), and ^{19}F (top right) NMR spectra of BuCzCF3*o*B (**5**) in $CDCl_3$.

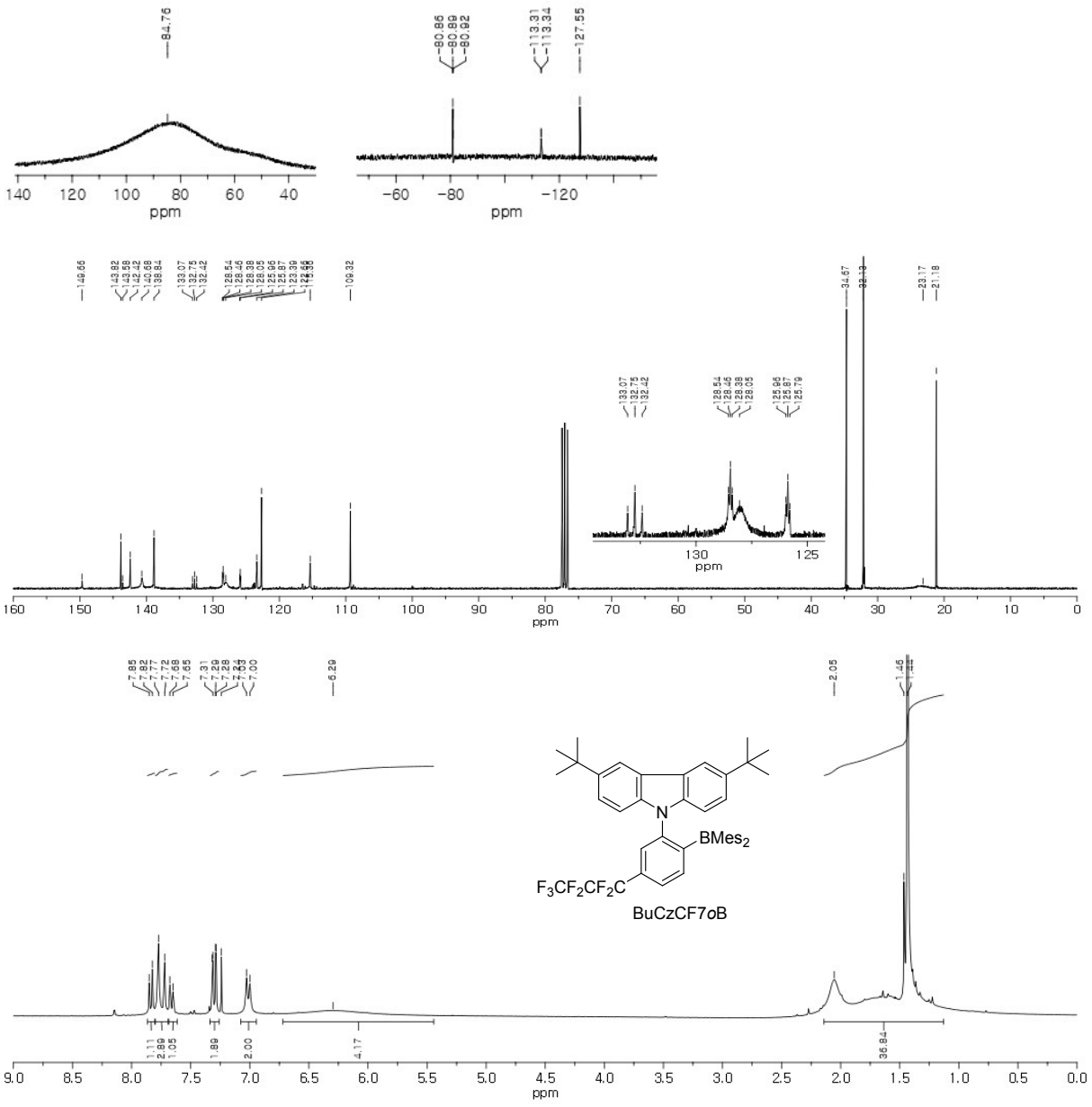

Figure S10. ^{1}H (bottom), ^{13}C (middle), ^{11}B (top left), and ^{19}F (top rght) NMR spectra of BuCzCF7*o*B (**6**) in $CDCl_3$.

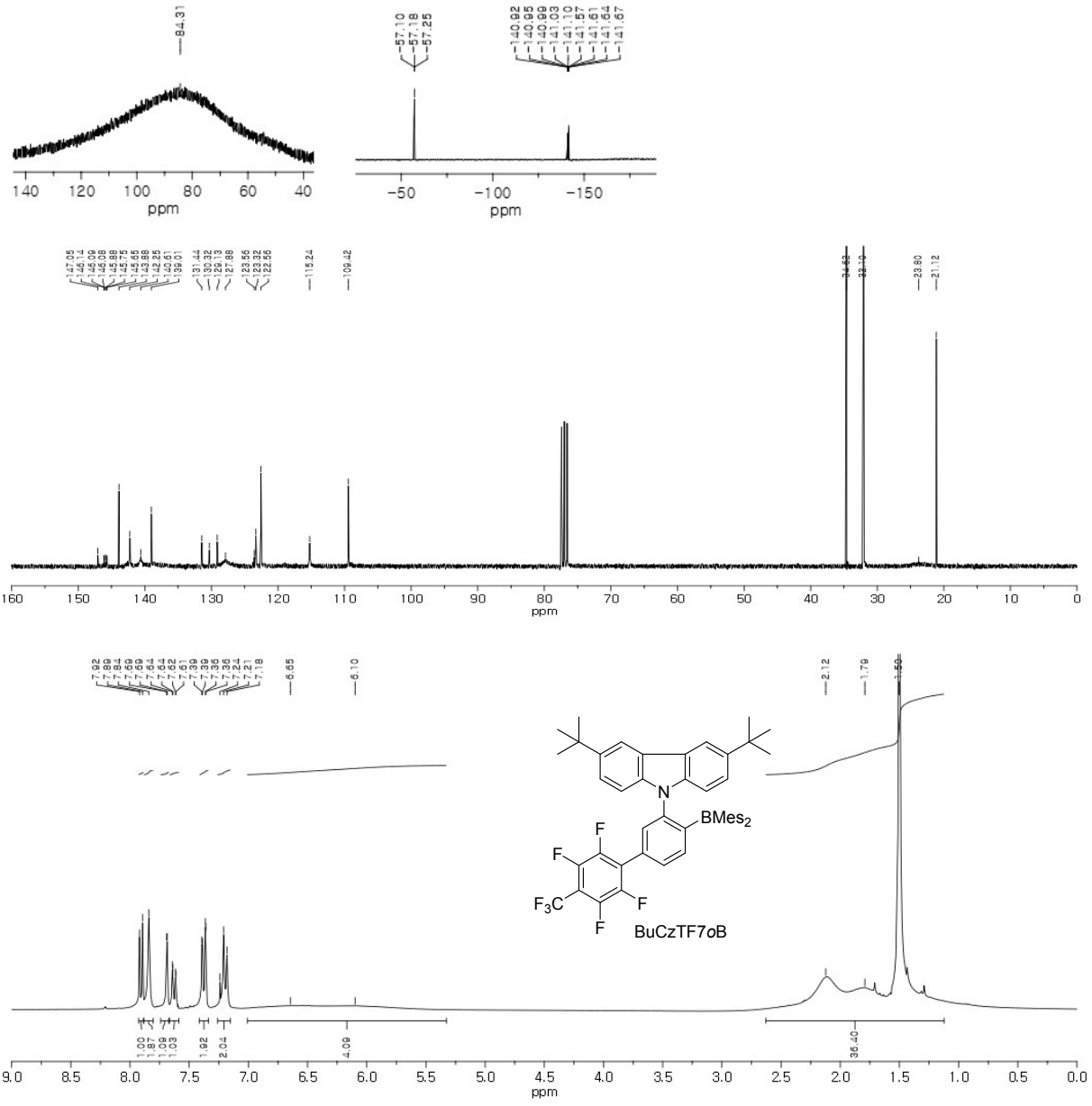

Figure S11. ^{1}H (bottom), ^{13}C (middle), ^{11}B (top left), and ^{19}F (top right) NMR spectra of BuCzTF7*o*B (**7**) in $CDCl_3$.

Table S1. Crystallographic data and parameters for **2** and **5**.

	2 (CzCF3*o*B)	**5** (BuCzCF3*o*B)
formula	$C_{37}H_{33}BF_3N$	$C_{45}H_{49}BF_3N$
formula weight	559.45	671.66
crystal system	Triclinic	Monoclinic
space group	*P–1*	$P2_1/c$
a (Å)	12.938(3)	21.878(5)
b (Å)	13.802(3)	12.963(3)
c (Å)	16.803(4)	13.676(3)
α (°)	89.688(11)	90
β (°)	86.924(12)	101.151(14)
γ (°)	84.560(11)	90
V (Å^3)	2982.88(12)	3805.43(15)
Z	4	4
ρ_{calc} (g cm^{-3})	1.246	1.172
μ (mm^{-1})	0.084	0.077
F(000)	1176	1432
T (K)	173(2)	173(2)
hkl range	−16 → +16, −17 → +17, −21 → +21	−27 → +29, −17 → +17, −18 → +18
measd reflns	52929	39103
unique reflns [R_{int}]	13615 [0.0369]	9424 [0.0464]
reflns used for refinement	13615	9424
refined parameters	757	451
R1[a] (I > 2σ(I))	0.0650	0.0731
wR2[b] all data	0.1818	0.1943
GOF on F^2	1.055	1.032
ρ_{fin} (max/min) (e Å^{-3})	0.466/−0.512	0.459/−0.387

[a] $R1 = \sum||Fo| - |Fc||/\sum|Fo|$. [b] $wR2 = \{[\sum w(Fo^2 - Fc^2)^2]/[\sum w(Fo^2)^2]\}^{1/2}$.

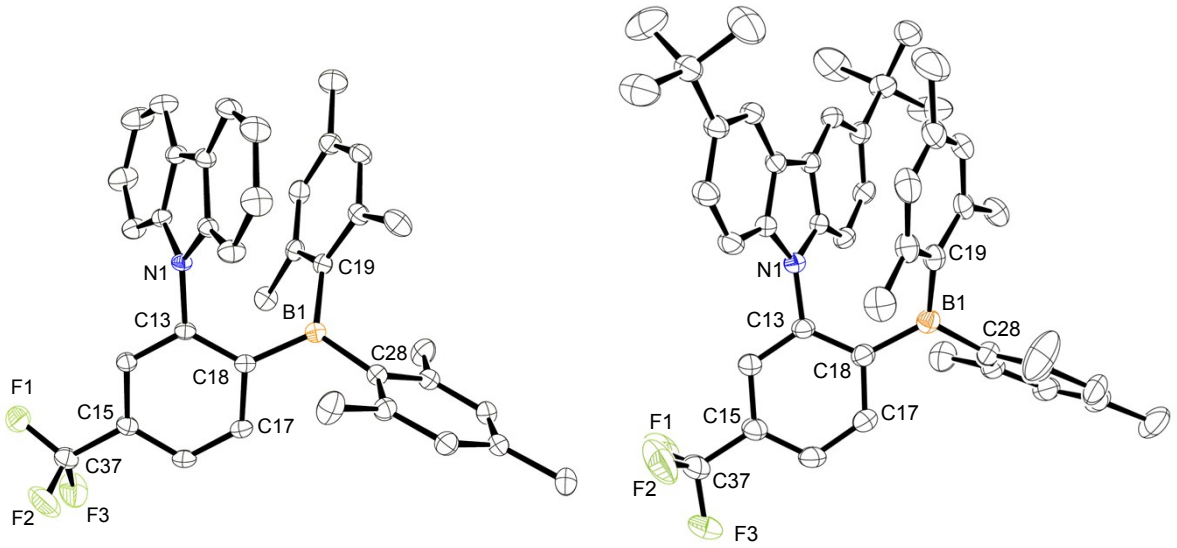

Figure S12. Crystal structures of **2** (left) and **5** (right) (40% thermal ellipsoids). The H-atoms are omitted for clarity.

Table S2. Selected bond lengths (Å) and angles (deg) for **2** and **5**.

	2	**5**
Lengths		
B(1)–C(18)	1.589(3)	1.588(3)
B(1)–C(19)	1.566(3)	1.569(3)
B(1)–C(28)	1.580(3)	1.586(3)
N(1)–C(13)	1.429(3)	1.426(3)
Angles		
C(18)–B(1)−C(19)	118.98(18)	120.95(19)
C(18)–B(1)−C(28)	119.18(18)	118.90(2)
C(19)–B(1)−C(28)	121.62(18)	120.00(2)
N(1)–C(13)−C(18)	121.83(17)	121.86(18)
C(13)–C(18)−B(1)	127.10(18)	127.73(19)
C(17)–C(18)−B(1)	115.88(18)	115.90(2)

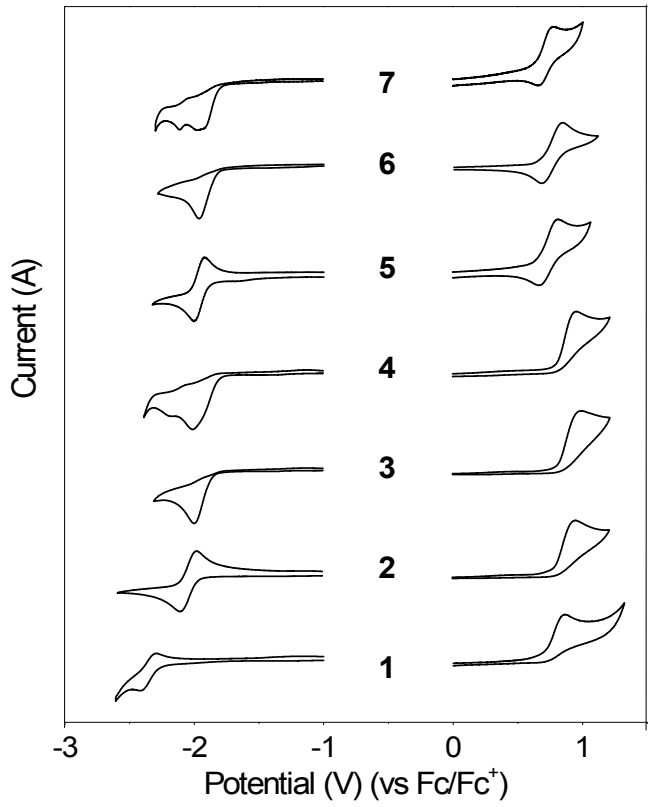

Figure S13. Cyclic voltammograms of **1**–**7** (1.0×10^{-3} M in DMF, scan rate = 200 mV/s).

Table S3. Electrochemical data for **1**–**7**.

Compound	Oxidation (V)	Reduction (V)	E_g (eV)
1 (Cz*o*B)	0.70[a]	−2.35[b]	3.05
2 (CzCF3*o*B)	0.79[a]	−2.04[b]	2.83
3 (CzCF7*o*B)	0.82[a]	−1.87[a]	2.69
4 (CzTF7*o*B)	0.81[a]	−1.81[a]	2.62
5 (BuCzCF3*o*B)	0.71[b]	−1.96[b]	2.67
6 (BuCzCF7*o*B)	0.76[b]	−1.83[a]	2.59
7 (BuCzTF7*o*B)	0.72[b]	−1.81[a]	2.53

[a]Irreversible (oxidation onset potential). [b]Reversible ($E_{1/2}$).

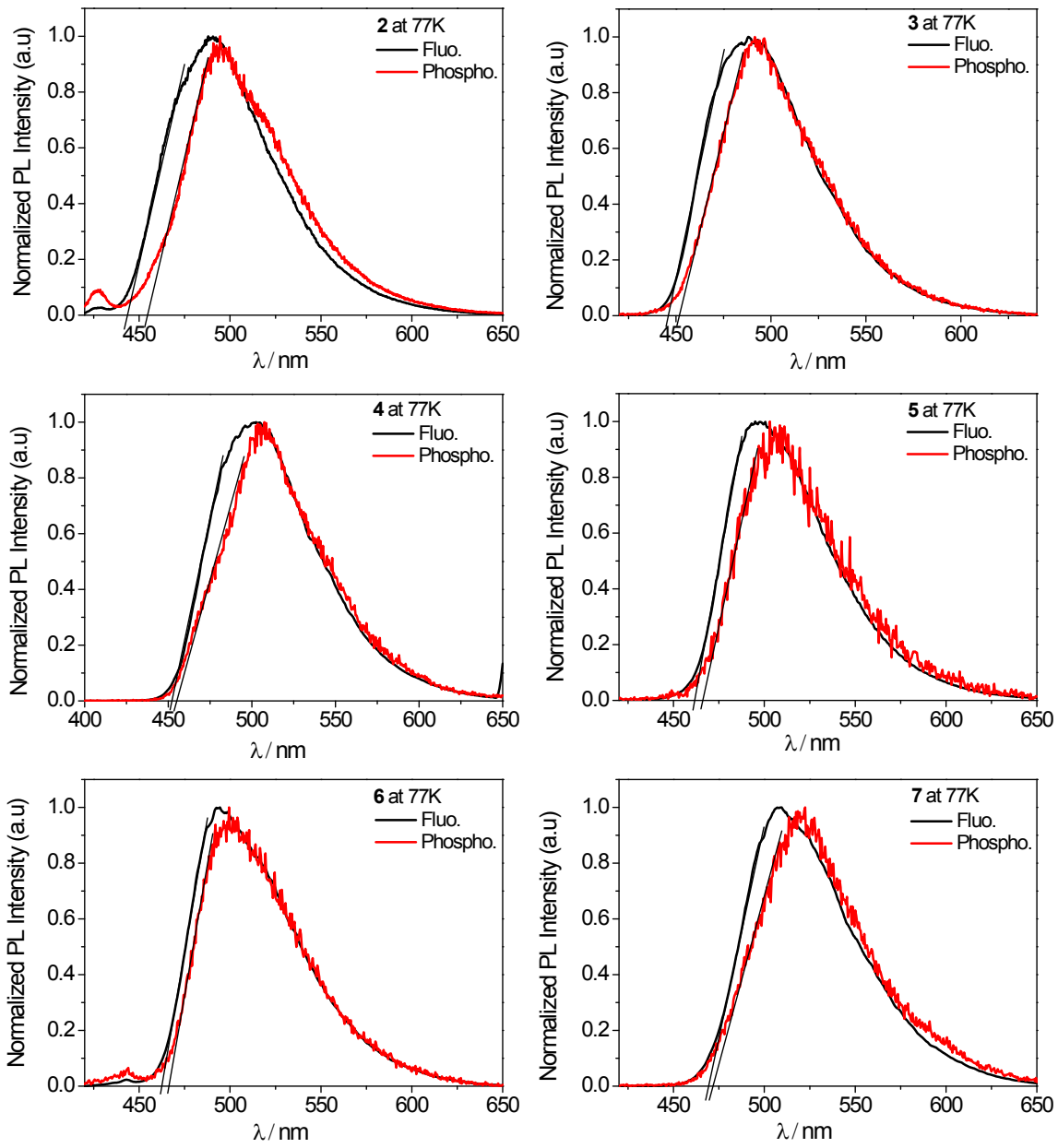

Figure S14. Fluorescence and phosphorescence spectra of *ortho* D–A compounds (**2**–**7**) in toluene at 77 K.

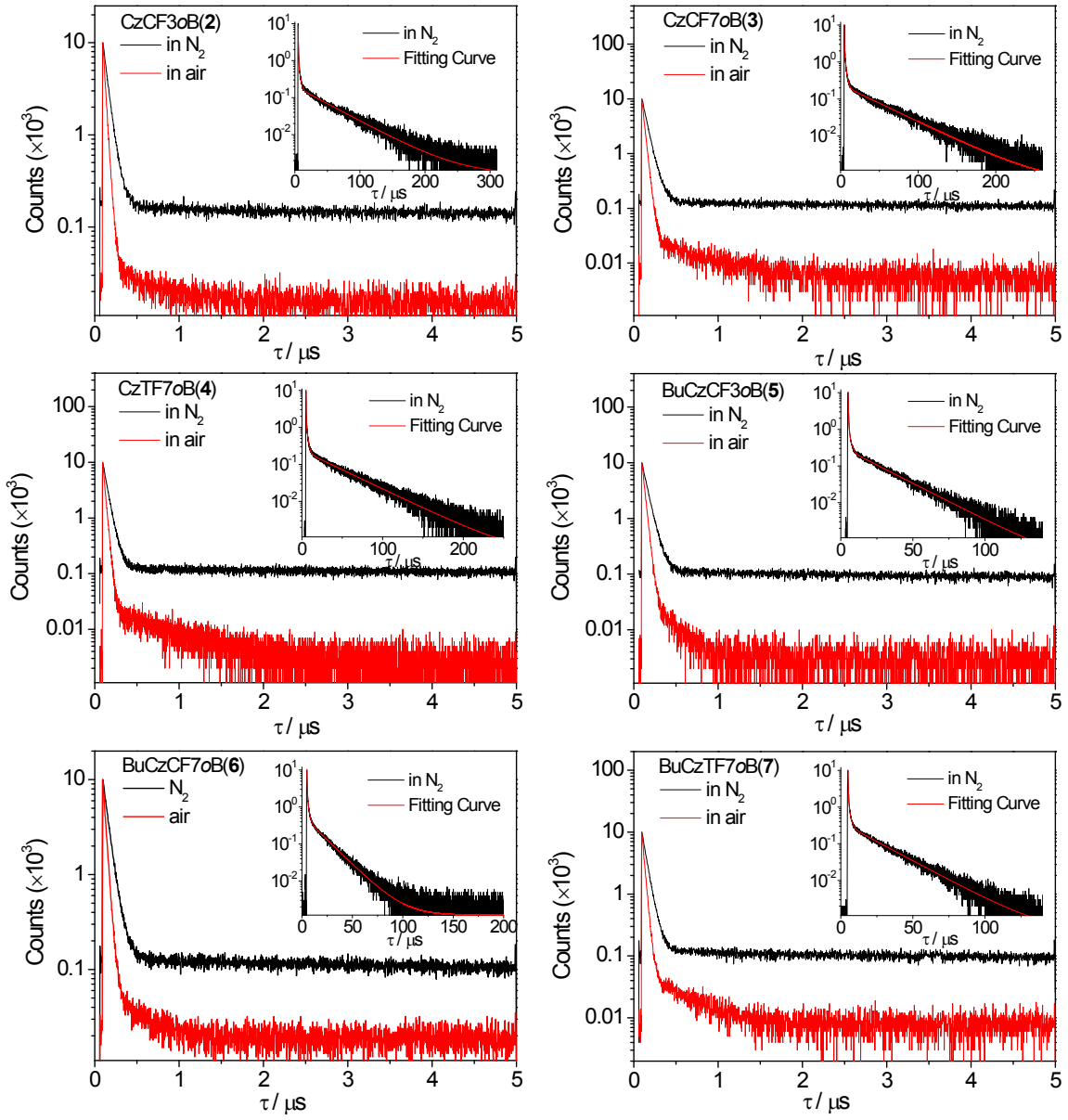

Figure S15. Transient PL decay curves of *ortho* D–A compounds (**2**–**7**) in oxygen-free toluene and air-saturated toluene from TCSPC mode at 298 K. Inset: the decay curve in oxygen-free toluene from MCS mode at 298 K.

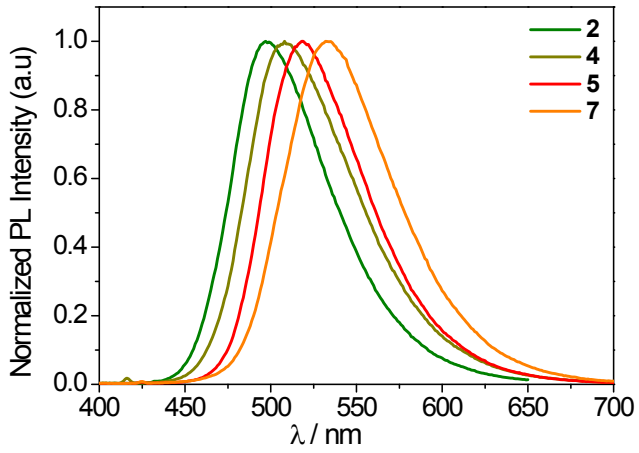

Figure S16. PL spectra of the host films (TCTA:B3PYMPM = 1:1) doped with 20 wt% of **2**, **4**, **5**, and **7**.

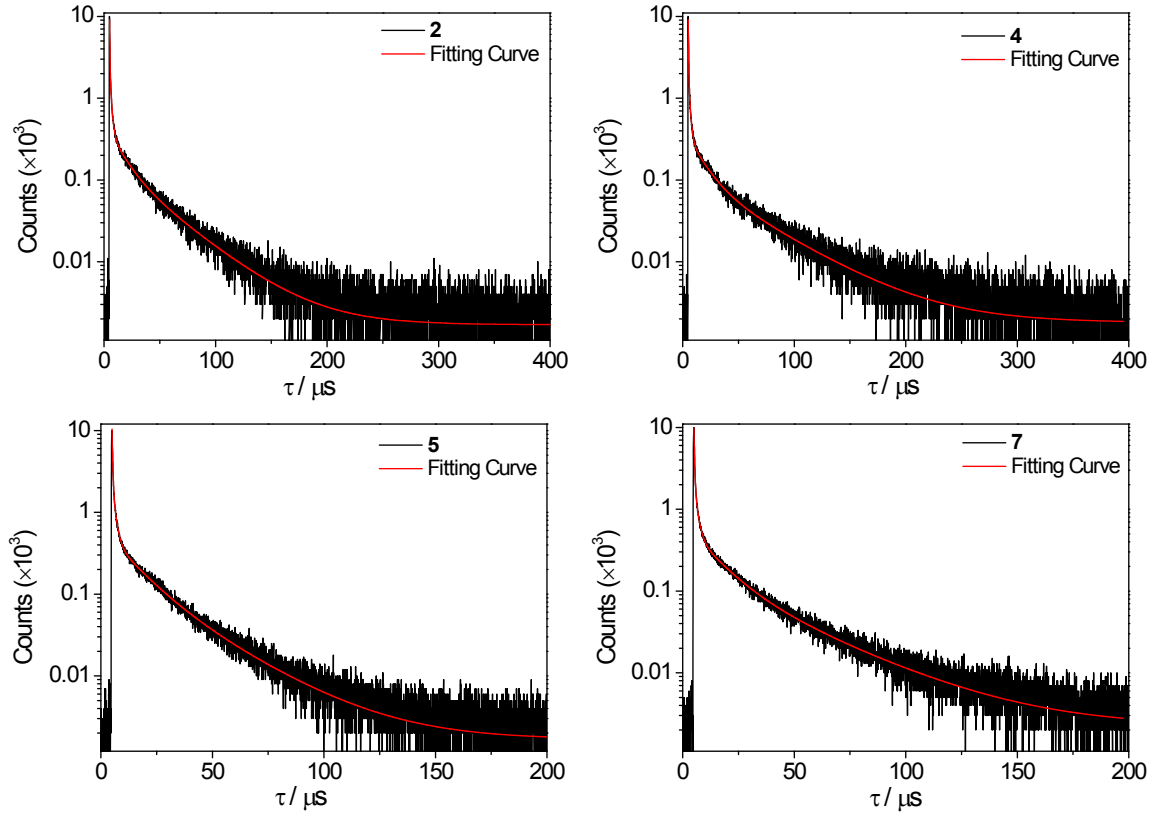

Figure S17. Transient PL decay curves of the host films (TCTA:B3PYMPM = 1:1) doped with 20 wt% of **2**, **4**, **5**, and **7** at 298 K.

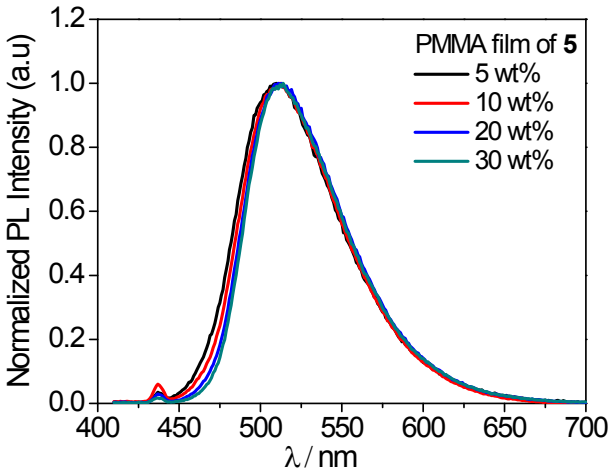

In PMMA (wt% of **5**)	λ_{PL} (nm)	PLQY (%)
5	508	81
10	510	85
20	511	91
30	511	87

Figure S18. PL spectra and PLQYs of the doped PMMA films with different concentrations of **5**.

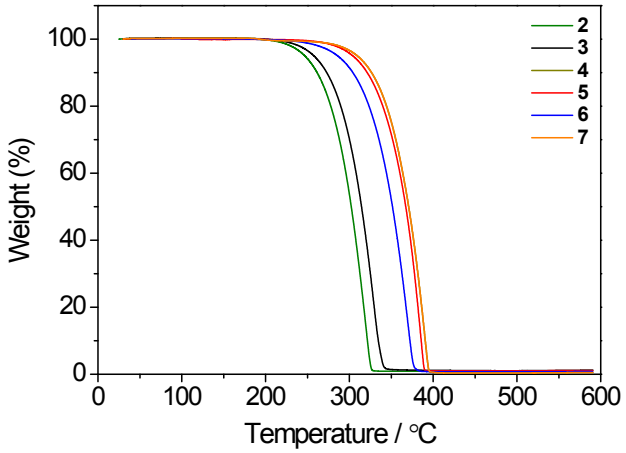

Figure S19. TGA curves of *ortho* D–A compounds (**2**–**7**).

2. Computational Results

Table S4. The contribution (in %) of donor and acceptor moieties to the frontier molecular orbitals and overlap integrals ($I_{H/L}$) between them for *ortho*-carbazole-appended triarylboron compounds (**1**, **2**, **4**, **5** and **7**). The introduced functional group (R^F) in the acceptor moieties are $–CF_3$ and $–C_6F_4CF_3$. All the numerical values are obtained using PBE0 (B3LYP) functional.

	MO	energy	donor	acceptor			$I_{H/L}$
		(eV)	(3,6-$(R)_2$-Cz)	Ph	R^F	$BMes_2$	
1 (Cz*o*B)	LUMO	−1.71	2.12	34.20	-	63.68	26.1
		(−1.79)	(1.46)	(33.82)	-	(64.72)	(24.3)
	HOMO	−5.62	89.51	5.29	-	5.20	
		(−5.37)	(90.28)	(4.56)	-	(5.16)	
2 (CzCF3*o*B)	LUMO	−2.00	1.99	40.07	2.37	55.57	25.6
		(−2.07)	(1.71)	(40.28)	(2.51)	(55.50)	(24.2)
	HOMO	−5.75	90.20	4.88	0.10	4.82	
		(−5.47)	(90.59)	(4.21)	(0.10)	(5.10)	
4 (CzTF7*o*B)	LUMO	−2.16	1.39	37.13	26.33	35.15	25.4
		(−2.25)	(1.12)	(36.43)	(29.29)	(33.16)	(23.5)
	HOMO	−5.73	89.00	5.77	0.20	5.03	
		(−5.45)	(89.70)	(4.96)	(0.18)	(5.16)	
5 (BuCzCF3*o*B)	LUMO	−1.98	2.09	40.03	2.39	55.49	24.2
		(−2.05)	(1.72)	(40.09)	(2.52)	(55.67)	(22.7)
	HOMO	−5.53	92.80	4.62	0.09	2.49	
		(−5.27)	(92.96)	(3.92)	(0.10)	(3.02)	
7 (BuCzTF7*o*B)	LUMO	−2.14	1.16	36.89	26.61	35.34	24.2
		(−2.23)	(1.15)	(36.13)	(29.84)	(32.88)	(22.4)
	HOMO	−5.51	91.60	5.56	0.17	2.67	
		(−5.25)	(92.03)	(4.79)	(0.15)	(3.03)	

Table S5. The calculated absorption wavelength (λ_{abs}, in nm) and the corresponding oscillator strength (f) for *ortho*-carbazole-appended triarylboron compounds. All the numerical values are obtained using PBE0 (B3LYP) functional.

	λ_{abs}	f_{abs}	Major contribution
1 (Cz*o*B)	408 (428)	0.0073 (0.0065)	HOMO → LUMO (97.6 (98.6))
2 (CzCF3*o*B)	431 (456)	0.0068 (0.0060)	HOMO → LUMO (98.1 (98.9))
4 (CzTF7*o*B)	448 (479)	0.0121 (0.0100)	HOMO → LUMO (97.0 (98.0))
5 (BuCzCF3*o*B)	457 (483)	0.0088 (0.0078)	HOMO → LUMO (98.5 (99.1))
7 (BuCzTF7*o*B)	477 (510)	0.0121 (0.0101)	HOMO → LUMO (97.4 (98.2))

Table S6. The calculated emission wavelength (λ_{em}, in nm) and the corresponding oscillator strength (f) for *ortho*-carbazole-appended triarylboron compounds. All the numerical values are obtained using PBE0 (B3LYP) functional.

	λ_{em}	f_{em}	Major contribution
1 (Cz*o*B)	478 (501)	0.0120 (0.0083)	HOMO → LUMO (98.2 (99.1))
2 (CzCF3*o*B)	534 (571)	0.0780 (0.0055)	HOMO → LUMO (98.5 (99.3))
4 (CzTF7*o*B)	573 (626)	0.0096 (0.0060)	HOMO → LUMO (98.1 (98.9))
5 (BuCzCF3*o*B)	575 (621)	0.0070 (0.0051)	HOMO → LUMO (99.0 (99.4))
7 (BuCzTF7*o*B)	624 (689)	0.0080 (0.0050)	HOMO → LUMO (98.5 (99.0))

3. Electroluminescence Results

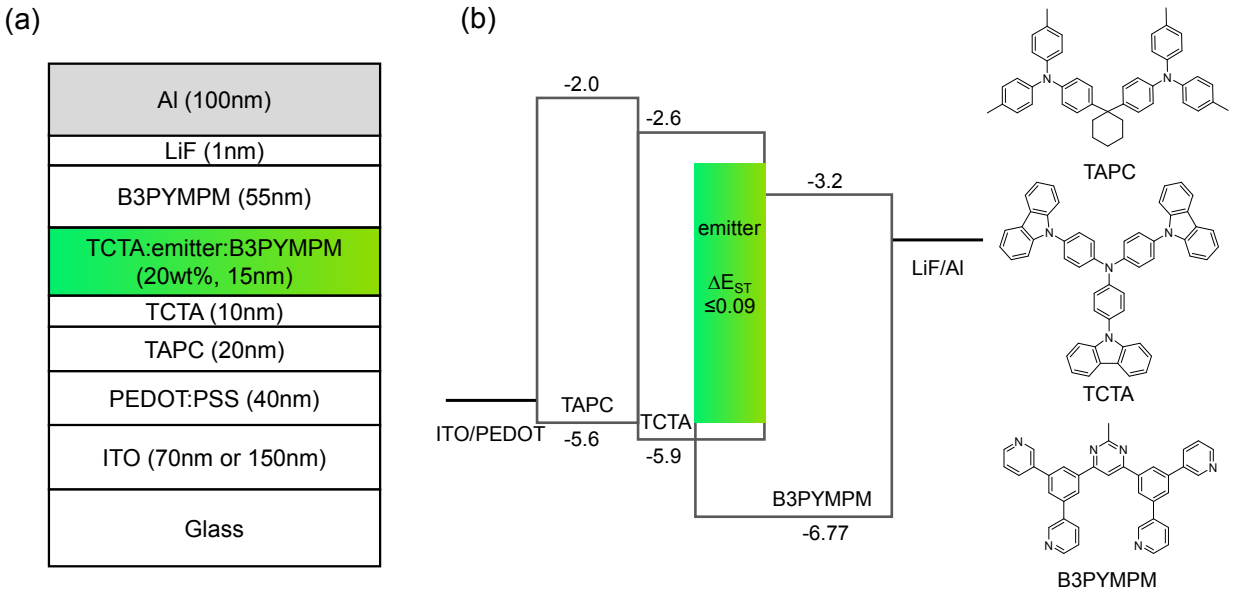

Figure S20. (a) Device structure of the proposed TADF-OLEDs. (b) Energy level diagrams of each device (in eV) relative to the vacuum level.

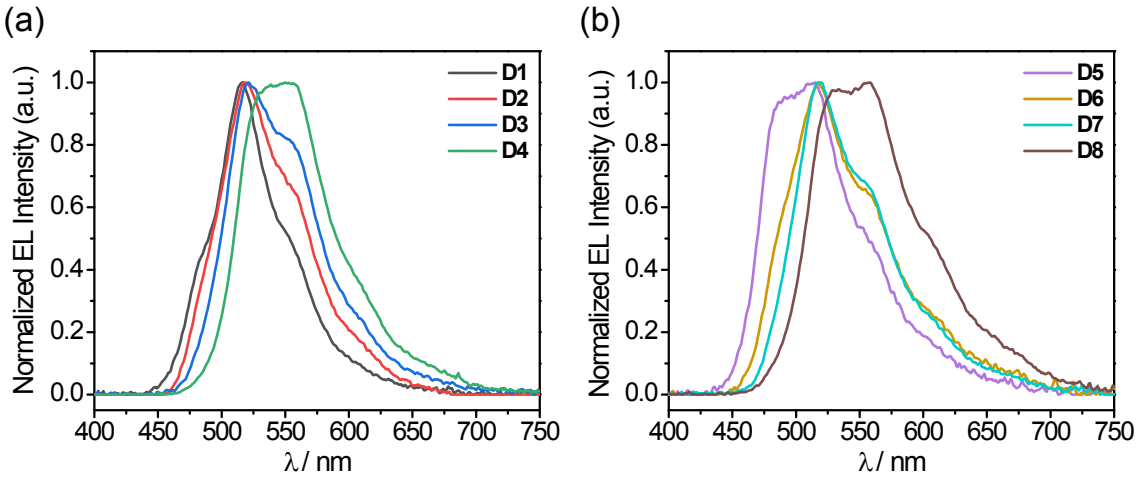

Figure S21. EL spectra of (a) **D1**–**D4** and (b) **D5**–**D8** fabricated with proposed TADF emitters (**2**, **4**, **5**, **7**).

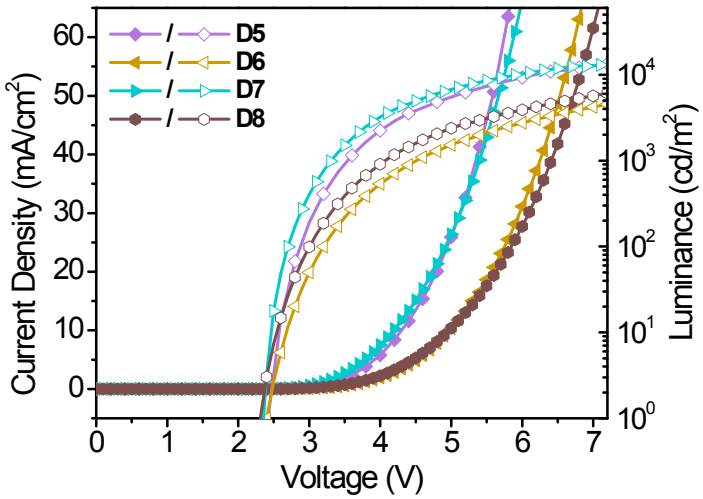

Figure S22. Current density−voltage−luminance (*J*−*V*−*L*) characteristics of devices (**D5**−**D8**).

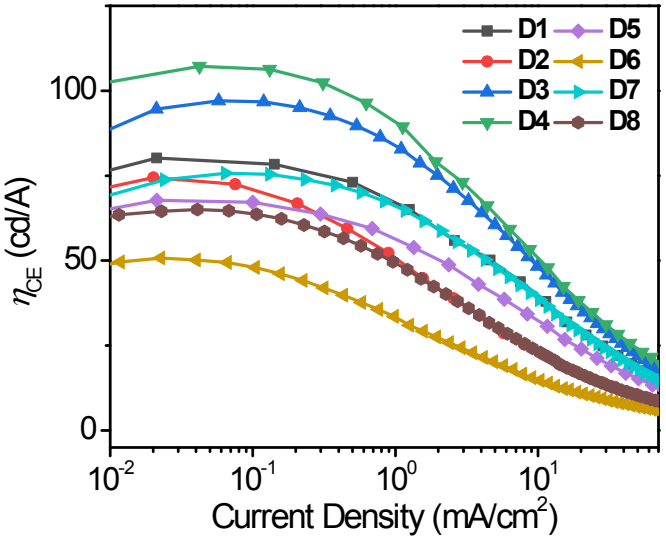

Figure S23. Current efficiency-current density (CE–*J*) characteristics of devices (**D1**–**D8**).

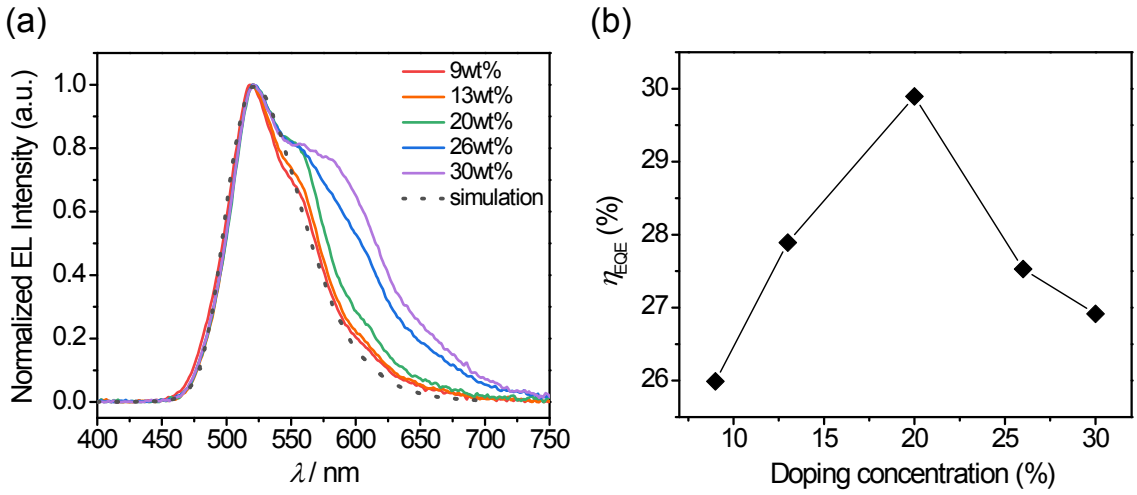

Figure S24. (a) EL spectra and (b) max. EQE of devices fabricated with various doping concentrations of BuCzCF3*o*B (**5**).

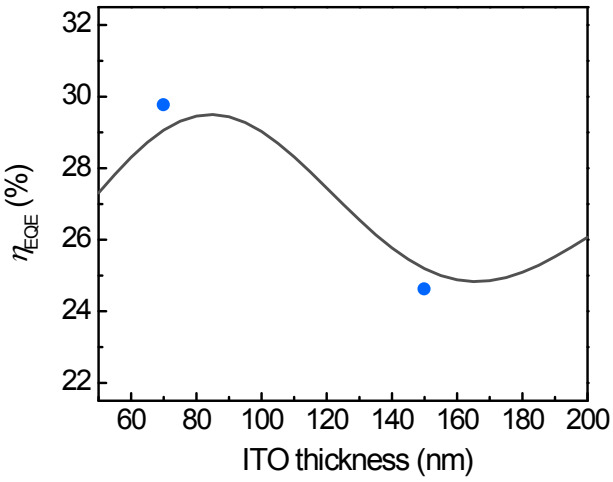

Figure S25. Simulated max. EQE as a function of ITO thickness at the horizontal transition dipole ratio of Θ = 0.76. The blue circles indicate the experimental max. EQE at ITO thickness of 70 and 150 nm.

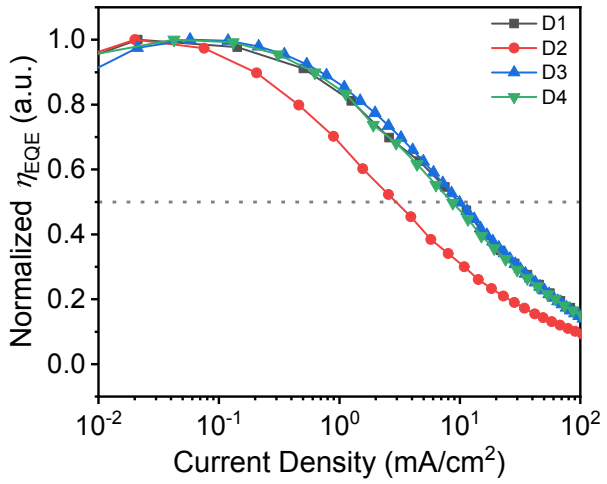

Figure S26. Normalized external quantum efficiency-current density (normalized η_{EQE}–*J)* curve of devices **(D1–D4)**.

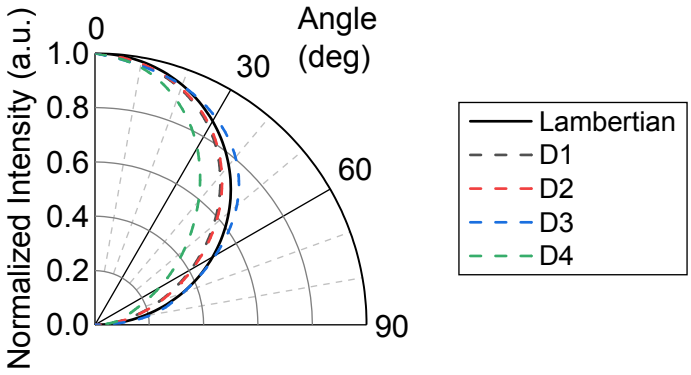

Figure S27. Normalized angular electroluminescence (EL) intensity of devices **(D1–D4)**.

Table S7. The performances of the boron-based TADF-OLEDs (EQE > 20%).

No.	Compound code	λ_{EL} (nm)	CIE (x, y)	EQE_{max} (%)/ PE_{max} (lmW^{-1})	Ref.
1	BuCzCF3*o*B (**5**)	521	(0.330, 0.598)	**29.9**/**123.9**	This work
2	MCz-BSBS	484	(0.14, 0.33)	25.9/54.6	*ACS Mater. Lett*. **2020**, *1*, 28
3	M3CzB	478	(0.14, 0.26)	**30.7**/-	10.1039/C9TC05950D
4	OBA-BrO	500	(0.21, 0.38)	22.5/56.9	*J. Mater. Chem. C* **2019**, *7*, 11953
5	*t*-DABNA	445	(0.13, 0.15)	**31.4**/33.6	*J. Mater. Chem. C* **2019**, *7*, 3082
6	ADBNA-Me-Tip	481	(0.11, 0.29)	21.4/-	*Org. Lett.* **2019**, *21*, 9311
7	2F-BN	501	(0.16, 0.60)	22.0/69.8	*Angew. Chem. Int. Ed*. **2019**, *58*, 16912
8	3F-BN	499	(0.20, 0.58)	22.7/72.3	
9	4F-BN	493	(0.12, 0.48)	21.9/51.3	
10	*ν*-DABNA	467	(0.12, 0.11)	**34.4**/-	*Nat. Photon.* **2019**, *13*, 678
11	TDBA–DI	-	(0.15, 0.28)	**38.15**/57.22	*Nat. Photon.* **2019**, *13*, 540
12	TDBA-Ac	448	(0.15, 0.06)	25.57/25.41	
13	PXB-DI	-	(0.16, 0.34)	**37.4**/	*ACS Appl. Mater. Interfaces* **2019**, *11*, 4909
14	PxzAZB	512	(0.26, 0.57)	27.5/80.6	*ACS Appl. Mater. Interfaces* **2019**, *11*, 10768
15	*p*-AC-DBNA	488	(0.17, 0.36)	20.5/42.5	*Adv. Opt. Mater.* **2019**, *7*, 19001302
16	BuCzMe*o*B	479	(0.135, 0.266)	**32.8**/	*Adv. Opt. Mater.* **2018**, *6*, 1800385
17	BuCz*o*B	480	(0.142, 0.344)	26.1/	
18	PXZPBM	505	(0.247, 0.543)	22.6/50.0	*ACS Appl. Mater. Interfaces* **2018**, *10*, 12886
19	MPAc-Bs	503	(0.20, 0.51)	25.3/77.4	*Adv. Funct. Mater*. **2018**, *28*, 1802031
20	TBN-TPA	474	(0.12, 0.19)	**32.1**/30.0	*Angew. Chem. Int. Ed.* **2018**, *57*, 11316
21	CzDBA	528	(0.31, 0.61)	**37.8**/121.6	*Nat. Photon.* **2018**, *12*, 235
22	*t*BuCzDBA	542	(0.37, 0.60)	**32.**4/109.8	
23	Cz*o*B	466	(0.139, 0.150)	22.6/	*ACS Appl. Mater. Interfaces* **2017**, *9*, 24035
24	DPA*o*B	502	(0.172, 0.488)	21.4/	
25	DABNA-2	469	(0.12, 0.13)	20.2/15.1	*Adv. Mater.* **2016**, *28*, 2777
26	**1**			21.7/	*Chem. Commun.* **2015**, *51*, 9443
27	**11**	503		22.1	*J. Mater. Chem. C* **2015**, *3*, 9122
28	**1**	502	(0.22, 0.55)	22.8/	*Angew. Chem. Int. Ed.* **2015**, *54*, 15231
29	**2**	492	(0.18, 0.43)	21.6/	

4. References

1. Lee, Y. H.; Jana, S.; Lee, H.; Lee, S. U.; Lee, M. H. *Chem. Commun.* **2018**, *54*, 12069-12072.

2. Lee, Y. H.; Park, S.; Oh, J.; Shin, J. W.; Jung, J.; Yoo, S.; Lee, M. H. *ACS Appl. Mater. Interfaces* **2017**, *9*, 24035-24042.

3. Sheldrick, G. M. *SHELXS-97: Program for the Solution of Crystal Structures* University of Göttingen, Germany, 2008.

4. Sheldrick, G. M. *Acta Crystallogr. A* **2008**, *64*, 112-122.

5. Adamo, C.; Barone, V. *J. Chem. Phys.* **1999**, *110*, 6158-6170.

6. Frisch, M. J.; Trucks, G. W.; Schlegel, H. B.; Scuseria, G. E.; Robb, M. A.; Cheeseman, J. R.; Scalmani, G.; Barone, V.; Petersson, G. A.; Nakatsuji, H.; Li, X.; Caricato, M.; Marenich, A. V.; Bloino, J.; Janesko, B. G.; Gomperts, R.; Mennucci, B.; Hratchian, H. P.; Ortiz, J. V.; Izmaylov, A. F.; Sonnenberg, J. L.; Williams-Young, D.; Ding, F.; Lipparini, F.; Egidi, F.; Goings, J.; Peng, B.; Petrone, A.; Henderson, T.; Ranasinghe, D.; Zakrzewski, V. G.; Gao, J.; Rega, N.; Zheng, G.; Liang, W.; Hada, M.; Ehara, M.; Toyota, K.; Fukuda, R.; Hasegawa, J.; Ishida, M.; Nakajima, T.; Honda, Y.; Kitao, O.; Nakai, H.; Vreven, T.; Throssell, K.; Montgomery Jr., J. A.; Peralta, J. E.; Ogliaro, F.; Bearpark, M. J.; Heyd, J. J.; Brothers, E. N.; Kudin, K. N.; Staroverov, V. N.; Keith, T. A.; Kobayashi, R.; Normand, J.; Raghavachari, K.; Rendell, A. P.; Burant, J. C.; Iyengar, S. S.; Tomasi, J.; Cossi, M.; Millam, J. M.; Klene, M.; Adamo, C.; Cammi, R.; Ochterski, J. W.; Martin, R. L.; Morokuma, K.; Farkas, O.; Foresman, J. B.; Fox, D. J. *Gaussian 16, Revision A.03*, Gaussian, Inc., Wallingford CT, 2016.

7. Becke, A. D. *J. Chem. Phys.* **1993**, *98*, 5648-52.

8. Tomasi, J.; Mennucci, B.; Cammi, R. *Chem. Rev.* **2005**, *105*, 2999-3094.

9. Gorelsky SI. AOMix: Program for Molecular Orbital Analysis, version 6.94, 2018. http://www.sg-chem.net.

10. Lu, T.; Chen, F. *J. Comput. Chem.* **2012**, *33*, 580-592.

11. Song, J.; Kim, K.-H.; Kim, E.; Moon, C.-K.; Kim, Y.-H.; Kim, J.-J.; Yoo, S. *Nat. Commun.* **2018**, *9*, 3207.

12. Moon, C.-K.; Kim, S.-Y.; Lee, J.-H.; Kim, J.-J. *Opt. Express* **2015**, *23*, A279-A291; Furno, M.; Meerheim, R.; Hofmann, S.; Lüssem, B.; Leo, K. *Phys. Rev. B* **2012**, *85*, 115205; Neyts, K. A. *J. Opt. Soc. Am. A* **1998**, *15*, 962-971; Barnes, W. L. *J. Mod. Opt.* **1998**, *45*, 661-699.